AD

USAAVLABS TECHNICAL REPORT 66-37

INVESTIGATION OF HIGH GAS TEMPERATURE UTILIZATION FOR ADVANCED TIP TURBINE FANS

By

M. R. Simonson

August 1966

U. S. ARMY AVIATION MATERIEL LABORATORIES
FORT EUSTIS, VIRGINIA

CONTRACT DA 44-177-AMC-218(T)
GENERAL ELECTRIC COMPANY
CINCINNATI, OHIO

Disclaimers

The findings in this report are not to be construed as an official Department of the Army position, unless so designated by other authorized documents.

When Government drawings, specifications, or other data are used for any purpose other than in connection with a definitely related Government procurement operation, the United States Government thereby incurs no responsibility nor any obligation whatsoever; and the fact that the Government may have formulated, furnished, or in any way supplied the said drawings, specifications, or other data is not to be regarded by implification or otherwise as in any manner licensing the holder or any other person or corporation, or conveying any rights or permission, to manufacture, use, or sell any patented invention that may in any way be related thereto.

Disposition Instructions

Destroy this report when no longer needed. Do not return it to the originator.

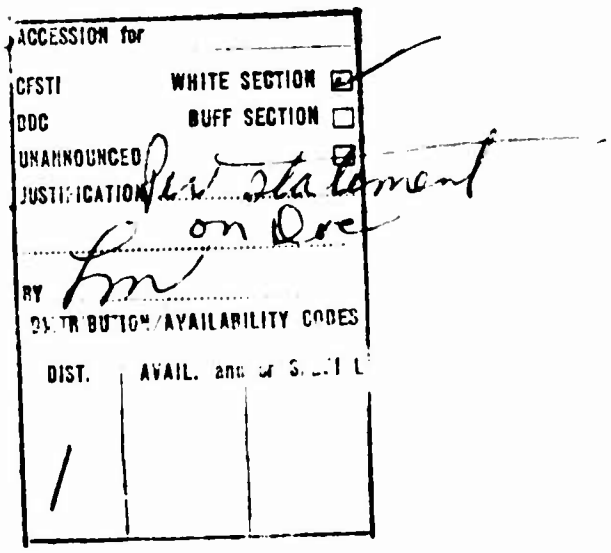

DEPARTMENT OF THE ARMY
U. S. ARMY AVIATION MATERIEL LABORATORIES
FORT EUSTIS, VIRGINIA 23604

This report is published for the dissemination of data pertaining to tip-turbine fans and ducting operating at gas temperatures commensurate with anticipated gas generator technology of the 1970 - 1975 time frame. The results contained herein appear to be feasible.

Task 1M121401D14415
Contract DA 44-177-AMC-218(T)
USAAVLABS Technical Report 66-37
August 1966

INVESTIGATION OF HIGH GAS TEMPERATURE UTILIZATION FOR ADVANCED TIP TURBINE FANS

by

M.R. Simonson

Prepared by

General Electric Company
Flight Propulsion Division
Advanced Technology and Demonstrator Programs Department
Lift Fan Systems Operation
Cincinnati, Ohio

for

U.S. ARMY AVIATION MATERIEL LABORATORIES
FORT EUSTIS, VIRGINIA

SUMMARY

Studies made of cooling systems for tip-turbine cruise fans are discussed. These studies include a review of planned and predicted core engine exhaust gas conditions; the conceptual design and evaluation of several turbine bucket-carrier cooling systems; sandwich-type double-wall duct constructions; and the definition of advanced material and future test program requirements.

CONTENTS

ILLUSTRATIONS

TABLES

SYMBOLS

c_p	specific heat, Btu per pound
g	gravitational constant, feet per second^2
h	convection coefficient, Btu/(hr-ft^2-°F)
J	778.26 ft-lb/sec per Btu/sec
K	a constant
k	thermal conductivity, Btu/(hr-ft-°F)
N	rotational speed, revolutions per minute
P	static pressure, pounds per square inch absolute
$P_{5.1}$	core engine exit pressure, pounds per square inch absolute
$P_{5.4}$	fan turbine inlet pressure, pounds per square inch absolute
$P_{S5.5}$	fan turbine exit static pressure, pounds per square inch absolute
P_n	Prandtl number
R_1	gas velocity relative to bucket, feet per second
R_n	Reynolds number
r	radius, inches
s	length of thin fin, inches
T_a	temperature at point (a), degrees Fahrenheit
T_b	temperature at point (b), degrees Fahrenheit
T_c	internal air temperature of buckets and carrier, degrees Fahrenheit
T_h	temperature outside of carrier, degrees Fahrenheit
T_{rail}	side rail temperature, degrees Fahrenheit
T_{tang}	tang temperature, degrees Fahrenheit
T_{TB}	bucket relative temperature, degrees Fahrenheit

T'_{TB}	bucket relative temperature, degrees Rankine
$T_{5.1}$	core engine exit temperature, degrees Fahrenheit
$T_{5.4}$	fan turbine inlet temperature, degrees Fahrenheit
$T'_{5.4}$	fan turbine inlet temperature, degrees Rankine
t	thickness of thin fin, inches
U	bucket peripheral velocity
U_{ft}	fan tip speed, feet per second
U_{tp}	turbine pitch line wheel speed, feet per second
V_1	nozzle exit velocity, feet per second
V_{a_1}	nozzle exit axial velocity, feet per second
V_{u_1}	nozzle exit tangential velocity, feet per second
W_B	bucket weight including box and shroud, pounds
W_P	side plate weight, pounds
W_R	side rail weight, pounds
W_S	seal weight, pounds
W_T	tang weight, pounds
X	thermal conductance per inch of length, Btu/(hr-in-°F)
x	distance, feet
α	nozzle exit gas angle, degrees
γ	specific heat ratio
η_c	cooling effectiveness
$\eta_{c_{plate}}$	cooling effectiveness for side plate
$\eta_{c_{tang}}$	cooling effectiveness for tang
η_N	nozzle efficiency

ρ	density, pounds per foot^3
σ	stress, pounds per square inch
σ_a	allowable design stress, pounds per square inch
μ	absolute viscosity, pounds per foot-second

BLANK PAGE

INTRODUCTION

This report describes results of conceptual design and analytical studies undertaken to determine payoff of turbine and gas duct component cooling methods applied to high-bypass remote-tip-turbine cruise fan systems.

This program was a second phase of U.S. Army Contract DA 44-177-AMC-218(T). The fundamental purpose of the first phase was to compare several concepts of high-speed and low-speed cruise fan propulsion systems, through parametric and preliminary design studies and application studies in typical U.S. Army vehicles. These results are reported in Reference 4.

Phase I showed that increased core engine exhaust gas temperature provides insignificant gain in tip-turbine-system thrust/weight ratio due to the effect of higher metal temperature on uncooled static and rotating turbine component weights. Phase II studies were therefore undertaken to determine the payoff of various turbine cooling methods in terms of weight and complexity and to provide conceptual designs of self-contained cooling systems.

The first step in this study was to review planned advanced engine programs to define exhaust gas characteristics which may be available as power sources for advanced tip-turbine fans. Of primary importance are the exhaust gas pressure and temperature and the fan tip speeds which may be required of advanced tip-turbine fans.

The second step was to conduct conceptual design studies to define several possible turbine rotor cooling systems and sandwich-type duct construction techniques applicable to scrolls, ducts and other static parts. After these systems were conceived, it was found necessary to make certain aerodynamic and heat transfer analyses of various component parts in order that a comparative evaluation could be made.

Finally a comparative evaluation was made of different cooling schemes on the basis of weight and complexity. Also, sandwich-type duct construction was compared to single-wall construction and the temperature pressure regimes determined where each is superior in terms of weight.

Lastly, requirements for advanced materials and component test programs were defined.

DEFINITION OF ADVANCED FAN TURBINE POWER SOURCES

A review of planned and predicted engine programs was conducted to define exhaust gas properties which may be available as power sources for advanced tip-turbine fans. This study covered the time period from 1963 to 1970, based on the date of core engine demonstration. In addition, an estimate was made of an engine cycle which may be typical of technology beyond 1970.

Exhaust gas characteristics of these engines are shown in Table I. It should be noted that demonstration dates ordinarily precede engine operational status by several years.

Table II gives a summary of a number of parameters significant to the duct and turbine design for fans driven by advanced core engines. Column 2 gives the ratio of fan tip-turbine total pressure to static pressure. This pressure ratio assumes an 8-percent drop in total pressure between the engine discharge and the fan turbine inlet and a turbine discharge static pressure of 15.3 pounds per square inch absolute. These values are typical of a tip-turbine-driven fan installation.

Column 3 gives the tangential components of the turbine nozzle spouting velocity, V_{ul}, based on the above pressure ratio and engine discharge temperature. A turbine nozzle exit angle of 20 degrees was assumed, since previous tip-turbine designs have not varied from this by more than plus or minus 2 degrees. For a tip turbine to achieve a reasonable efficiency, its pitch line wheel speed must not be less than 0.44 or 0.45 times V_{ul}. Thus, if a ratio between fan tip diameter and turbine pitch line diameter is assumed, an estimate of the minimum fan tip speeds required for these engine cycles can be made. If the fan tip diameter is assumed to be 0.92 times the turbine pitch line diameter, column 4 gives fan tip speeds, U_{ft}, corresponding to a value of U_{tp}/V_{ul} equal to 0.45. These are the minimum tip speeds required by the tip turbine. High pressure ratio fans may require tip speeds in excess of these values.

Tip-turbine buckets do not see the full engine exhaust gas temperature because of the temperature drop through the nozzle vanes and the relative velocity of the turbine buckets. Figure 1 shows the ratio of bucket relative total temperature to turbine inlet temperature as a function of turbine pressure ratio and U_{tp}/V_{ul}. Column 5 of Table II gives bucket relative total temperature for these engine cycles at a value of 0.45 for U_{tp}/V_{ul}. It is seen from Figure 1 that if the fan tip speed, and thus U_{tp}/V_{ul}, must be higher than the values shown in column 4, then the bucket relative temperatures will be reduced somewhat. A derivation of the relations given in Figure 1 is given in Appendix I.

TABLE I
ADVANCED CORE ENGINE EXHAUST GAS CHARACTERISTICS

Engine	$T_{5.1}$ °F	$P_{5.1}$ PSIA	Specific $\frac{HP}{lb/sec}$	Demonstration Date
A	1227	41.1	157.2	1965
B	1290	39.8	149.7	1965
C	1343	56.6	201.4	1966
D	1387	52.6	196.6	1963
E	1334	38.2	148.4	1968
F	1737	45.2	210.9	1968
G	1634	58.0	236.3	1968
H	1586	60.9	239.7	1968
I	1667	45.7	205.5	1968
J	1620	74.0	270.8	1970+

TABLE II
TIP-TURBINE PARAMETERS MATCHING ADVANCED CORE ENGINE CYCLES

Engine	$P_{5.5}/15.3$	V_{ul} ft/sec	U_{ft} ft/sec	T_{TB} °F
A	2.47	2001	828	1022
B	2.20	1916	793	1104
C	3.13	2293	950	1076
D	2.91	2254	970	1128
E	2.12	1904	788	1151
F	2.50	2295	951	1467
G	3.21	2495	1034	1318
H	3.37	2509	1038	1267
I	2.53	2276	942	1384
J	4.45	2543	1054	1232

For the design of scrolls and ducts for tip turbines, it is important to know required duct sizes in addition to the gas pressures and temperatures. In past designs, it has been found that the duct Mach numbers cannot exceed about 0.3 without incurring excessive total pressure losses. A useful parameter obtains from the product of exhaust gas pressure, $P_{5.1}$, and duct diameter in inches, sized for a Mach number of 0.3; this quantity determines the hoop loading in the duct skin.

If core engine compressor bleed air is required for cooling cruise fan components, its effect on core engine performance should be evaluated. An analysis was made of each of the advanced core engine cycles to determine the effect of compressor discharge bleed on its ideal exhaust specific horsepower and its specific fuel consumption. As air is bled from the compressor discharge station of an engine, the cycle pressure ratio will drop unless either the cycle temperature is increased or the turbine resized for a lower flow.

In this analysis, the cycle temperature was assumed fixed. The case where the turbine was not resized and the cycle pressure ratio was allowed to drop was investigated. Also, the case where the turbine was resized to maintain the original cycle pressure ratio was investigated. The results of this analysis are presented in Tables III and IV in terms of specific horsepower derivatives and specific fuel consumption derivatives. These derivatives are defined as follows:

$$\text{SHP Derivative} = \frac{\text{percent change in SHP}}{\text{change in percent of bleed flow}}$$

$$\text{SFC Derivative} = \frac{\text{percent change in SFC}}{\text{change in percent of bleed flow}}$$

The specific horsepower and percent of bleed are both based on engine inlet flow. The specific fuel consumption is defined by:

$$\text{SFC} = \frac{\text{fuel flow - lb/hr}}{\text{available exhaust horsepower}}$$

The case where cycle temperature is allowed to increase to maintain the pressure ratio without resizing of the turbine was also examined, but felt to be impractical because of the effect of higher temperatures on the turbine. This approach would, however, show much smaller performance penalties for bleed air extraction. If bleed air could be extracted at an intermediate pressure rather than at the compressor discharge station, the effect on core engine performance would also be somewhat less.

TABLE III
EFFECT OF BLEED AIR ON CORE ENGINE PERFORMANCE
WITH NO RESIZING OF TURBINE

Engine	Specific Horsepower Derivative (% SHP/% Bleed)	Specific Fuel Consumption Derivative (% SFC/% Bleed)
A	-2.78	2.05
B	-2.44	2.04
C	-2.36	1.69
D	-2.32	1.63
E	-2.50	1.80
F	-2.18	1.41
G	-2.18	1.45
H	-2.20	1.48
I	-2.21	1.45
J	-2.27	1.72

TABLE IV
EFFECT OF BLEED AIR ON CORE ENGINE PERFORMANCE
WITH TURBINE RESIZED FOR BLEED

Engine	Specific Horsepower Derivative (% SHP/% Bleed)	Specific Fuel Consumption Derivative (% SFC/% Bleed)
A	-2.99	1.99
B	-2.41	1.41
C	-2.48	1.48
D	-2.39	1.06
E	-2.48	1.39
F	-2.06	1.19
G	-2.19	1.25
H	-2.25	1.48
I	-2.12	1.12
J	-2.43	1.43

CONCEPTUAL DESIGN STUDIES

Tip-turbine cooling problems can be divided into three main areas: the ducting and scrolls, the turbine nozzle vanes, and the turbine bucket and carrier assembly. Temperatures downstream of the turbine rotor will generally be low enough that static parts in this area will not require cooling. Turbine nozzle vane cooling will be a necessity for temperatures above about 1600 degrees Fahrenheit, in order to achieve the long life required of cruise fans. In the temperature range between 1300 degrees Fahrenheit and 1600 degrees Fahrenheit, convection cooling of the vanes with fan air may pay off in terms of net weight savings. For temperatures above about 1650 degrees Fahrenheit, core engine bleed air will probably be required to film cool vane trailing edges. A brief investigation has shown that about 0.8 percent of core engine air would be required at 1700 degrees Fahrenheit and about 3.1 percent at 1800 degrees Fahrenheit to maintain trailing edge temperatures of 1600 degrees Fahrenheit.

Turbine vane nozzle cooling technology is well developed for conventional turbines, and there are no apparent problems peculiar to tip turbines in this area. On the other hand, cooling of ducting, scrolls, and tip-turbine bucket and carrier assemblies has not previously been investigated. For these reasons, conceptual design studies were conducted to find ways of constructing sandwich-type ducting for use in scrolls, ducts, and diverter valves, and to devise a number of schemes for cooling bucket and carrier assemblies.

Figure 2 shows one possible way of constructing sandwich-type ducting. This construction consists of a thin inside liner separated from an external wall by a ceramic fiber insulation material. The external wall is designed to contain the gas pressure, while the internal liner serves only to keep the insulation in place and is lowly stressed. The internal liner is made up of short overlapping sections and contains longitudinal convolutions so that it may freely expand and contract with variations in temperature. The external duct wall contains one circumferential convolution for each section of the liner. The liner is attached to the external wall by means of small bolts or rivets at the points where the convolutions in the liner and external wall cross. The bolts or rivets are insulated from the external wall in order to minimize heat conduction. However, there will still be hot spots on the outer wall at the attachment points, and it is intended that the convolutions will sufficiently relieve the thermal stresses at these points.

Figure 3 shows a second possible construction method for sandwich-type ducting. This construction also consists of a thin inside liner separated from an external wall by a ceramic fiber insulation material. In this construction, the inner liner is again made up of short overlapping sections free to expand longitudinally. However, instead of being attached to the outer wall, it is left free to expand or contract radially as well. The liner is held in by a flange at its upstream end, which is free to expand radially, as shown in Figure 3. This flange is restrained from axial motion

by a series of tabs attached about the outer wall of the duct. These tabs may also be insulated to minimize heat conduction to the outer wall. The outer wall is made in sections that are the same length as the liner sections. The sections can then be welded together as a unit after the insulation and liner have been installed in each section. This type of duct construction is probably better adapted for use in completely circular ducts rather than in scrolls or diverter valves because of the way in which the liner is retained.

In both of these duct designs, the outer walls are maintained at quite low temperatures, so that additional external insulation blankets should not be required. These low skin temperatures will also permit more freedom in the selection of materials for the outer walls and will minimize the need for bellows to take up thermal expansions.

There are a number of ways in which the turbine bucket and carrier assembly can be cooled. In this study, it was felt that it would not be necessary to use core engine compressor bleed air for bucket and carrier cooling. Efforts were concentrated on the following possibilities:

1. Conduction of heat to fan blade tips
2. Exclusion of hot gas from carrier area by either
    a. Cool fan discharge air or
    b. Hot turbine gas diluted by cool air
3. Shielding of critical areas from direct contact with hot gas
4. Internal cooling of bucket and carrier assembly with cool fan air

Figure 4 shows a tip turbine employing all of these cooling methods. Here, gas seals are added near the outer periphery of the carrier on both the forward and aft sides. On the forward side, the area between the inner and outer seals is vented to the nacelle exterior. At low forward flight speed, the static pressure at the fan tip is lower than either the turbine static pressure or the nacelle static pressure; thus, hot gas leakage from the turbine mixes with cool ambient air in the space between seals, and this warm mixture then flows into the fan. As forward flight speed increases, the ram effect tends to raise both the fan and turbine static pressures about equally, while the nacelle exterior static pressure tends to drop somewhat; thus, fan tip leakage flows into the seal space, cools the forward side of the carrier, mixes with the hot turbine leakage and flows overboard through ports on the nacelle exterior. With this arrangement, there is some intermediate flight speed where the fan tip static pressure is equal to the external nacelle pressure. At flight speeds near this point, hot turbine gas will flow both into the fan and through the overboard ports, since the turbine static pressure is higher than either. One solution to this problem is to have the seal space area vented to ram pressure until this intermediate speed range is exceeded. A valve arrangement would then automatically operate to vent the seal space to a low pressure area on the nacelle.

This cooling scheme has the advantage in the high flight speed regime, in that it eliminates hot gas flow into the fan tip forward of the rotor. This leakage has been estimated to cause about 2 percent loss in fan efficiency in previous fan designs.

Figure 4 shows the aft side of the bucket carrier cooled by fa discharge air ducted into the aft seal space area. Since the fan discharge pressure is higher than the static pressure on either the fan or the turbine side of the seal, leakage will always go into both the fan and turbine streams. Fan discharge air could be taken from ports on the pressure side of the fan stators, or from scoops located aft or between the fan stators.

Internal cooling of the carrier and buckets can be accomplished by mounting air scoops on the aft side of the bucket carrier, as shown in Figure 4. These scoops can force cool air into the interior of the carrier, up through the hollow bucket airfoils, and out the bucket tips. The total pressure of this cooling air is raised substantially by the scoops and by the centrifugal pumping action of the buckets. An alternative method of internal cooling is shown in Figure 5, where inducers, mounted between the fan rotor blade tips, force are into the interior of the carrier through openings in the fan tip shroud. This method could potentially improve fan performance by removing the inlet boundary layer just ahead of the fan rotor. A third alternative for internal cooling of the carrier, if the bucket airfoils need not be cooled, is shown in Figure 6. Here, the openings in the fan tip shroud, through which the blade tangs pass, are enlarged, allowing fan air to circulate from the pressure side of the fan blades, through the carrier, and out at the suction side of the fan blades. This scheme, however, would probably have some detrimental effect on fan tip performance. The bucket airfoils probably could not be internally cooled by this method, since the carrier internal pressure would be lower than the bucket tip static pressure.

Both Figures 4 and 5 show how a shield could be employed to prevent direct inpingement of hot turbine gas upon the bucket attachment area.

AERODYNAMIC AND HEAT TRANSFER ANALYSES

To evaluate the various conceptual designs and cooling schemes, it was necessary to conduct a number of aerodynamic and heat transfer analyses. In the analysis of the bucket and carrier assembly, it would have been impossible to make a completely general study, and it was decided to analyze in detail one specific configuration. This specific configuration was for a fan with a pressure ratio of 1.25, a tip speed of 940 feet per second, and a tip diameter of 56.7 inches. The fan was driven by engine "D", which is described in Tables I and II. It was felt that this bucket and carrier geometry would be reasonably representative of future cruise fan designs, except as modified for cooling requirements.

THERMAL CONDUCTANCE OF BUCKETS AND ATTACHMENTS

The bucket and its attachment structure form rather complicated heat flow paths between the hot turbine gas, bucket cooling air, and the carrier rail outer edges. Detailed temperature distributions in this structure were not of concern in this study, but it becomes necessary to know its overall equivalent thermal conductance in order to evaluate temperatures at more critical locations in the carrier assembly.

The bucket and attachment structure is exposed to three sources of heat: the turbine hot gas, the cooling air inside of the bucket airfoils, and the carrier rail outer edges. We will assume that cooling air on the outside fore and aft faces of the rails does not come in contact with the bucket attachment structure. We can also assume that the fore and aft bucket attachment areas can be treated separately because of the low thermal conductance of the thin interconnecting sheet metal structure. With these assumptions, the bucket and attachment structure can be idealized by an equivalent thermal network as shown in Figure 7. The conductances between the hot turbine gas and the cooling airflow, X_5 and X_6, will not need to be known for our purposes if we assume that the hot gas and cooling air temperatures are known. The conductances X_1, X_2, X_3, and X_4 were computed with and without cooling airflow and with and without shielding to cover the attachment area, as shown in Figure 4. These results are summarized in Table V. The basic geometry assumed in this analysis is shown in Figure 8. Only one-half of a bucket and carrier assembly is shown in this figure, since the carriers are symmetrical about the midspan location. The bucket and box structure are of 0.010-inch sheet, while the side rails and seals are of 0.015-inch sheet.

Convection coefficients on the outside of the buckets were calculated by using the following equation for turbulent boundary layer on a flat plate.

$$h = 0.029 \left(\frac{k}{x}\right) (R_n)^{0.8} (P_n)^{0.33}$$

where

$R_n = \sigma V x/\mu$

x = distance from leading edge and fluid properties are evaluated at mean film temperature.

For the specific configuration chosen for this analysis, the bucket surface velocities did not vary greatly over most of the chord length, and the following average conditions were used:

	Suction Side	Pressure Side
Surface velocity, feet per second	1839	1003
Film temperature, degrees Fahrenheit	1080	1200
Density, pound/foot^3	.0271	.0440
Viscosity, pound/foot/hour	.0914	.0958
Conductivity, Btu/(hour-foot-degrees Fahrenheit)	.0350	.0368
P_n	0.692	0.697

TABLE V
EQUIVALENT THERMAL CONDUCTANCES FOR BUCKET AND ATTACHMENT, Btu/(hr-in-°F)

Configuration	X_1	X_2	X_3	X_4
1. Shielded, Uncooled	.1720	0	.1702	0
2. Shielded, Cooled	.1446	.0210	.1310	.0233
3. Unshielded, Uncooled	.2329	0	.2245	0
4. Unshielded, Cooled	.1905	.0181	.1803	.0195

Bucket external convection coefficients were then calculated as a function of distance from the leading edge, x. The result is shown in Figure 9. To simplify the actual analysis, the average of the suction and pressure side convection coefficient was used and varied in a stepwise fashion along the blade surface. The convection coefficient between the buckets on the outer surface of the carrier was assumed to be equal to the bucket convection coefficient at the same axial location.

The underside of the side rail overhang was assumed to be exposed to hot gas for the unshielded cases. The convection coefficient for these areas was assumed to be 50 Btu/(hr-ft^2-°F). For the shielded cases, heat transfer was assumed to be zero on these areas.

For the cooled cases, it was assumed that the internal surfaces of the buckets were in contact with the cool air. A bucket internal convection coefficient of 50 Btu/(hr-ft^2-$^\circ$F) was assumed. It was estimated that a cooling airflow velocity of about 350 feet per second would produce this value in this configuration.

Actual heat transfer computations for this analysis were made on a digital computer using the "THTB" general heat transfer analysis program described in reference 3.

Although the values for the equivalent conductances of the bucket and attachment will be affected by changes in geometry and convection coefficients, it is felt that the values shown in Table V are sufficiently representative to be used for preliminary design purposes.

SIDE RAIL TEMPERATURE CALCULATIONS

Temperatures of the bucket-carrier side rails are important, since these parts are designed to their stress limit. Figure 10 shows locations of critical stress points on the carrier assembly. There are critical stress points at three locations on the carrier side rails. First, at point (a), the shear stress may reach a limit on either side of the side plate at about the mean rail radius. Second, the combined bending stress and radial tensile stress due to the bucket load may reach a limit at point (b), just below the bucket attachment area and on either side of the side plate. If the carrier has a second seal, the seal bending stress will also be a maximum at this point. Third, the combined shear stress and radial tensile stress due to the bucket load may reach a limit at point (c), just above the center of the side plate.

Because of the high thermal resistance of the thin sheet metal side rails, it is reasonable to assume that the rail temperature at point (a) is not influenced by conduction of the blade tang or conduction from the bucket attachment area. The temperature at point (a), then, is determined by only the air temperatures and convection coefficients on the two surfaces of the rail and may be calculated by the following equation:

$$T_a = T_h - \eta_c (T_h - T_c)$$

where

$$\eta_c = \frac{h_i}{h_i + h_o}$$

h_i = internal convection coefficient

h_o = external convection coefficient

T_c = internal cooling air temperature

T_h = external gas temperature

T_a = side rail temperature at pc (a)

The quantity η_c is usually referred to as the cooling effectiveness.

The external convection coefficient on the side rail may be estimated from the equation for the convection coefficient on the side of a rotating disk with turbulent boundary layer given in reference 1 as

$$h_o = \frac{.0742\ r^{0.6}\ (PN)^{0.8}}{(T_h + 460)^{0.6}}$$

where

r = radius in inches
P = static pressure in pounds per square inch absolute
N = rotational speed in revolutions per minute

For the specific confuguration selected for this analysis,

r = 28.5 inches
P = 14.7 pounds per square inch absolute
N = 4360 revolutions per minute

The above equation then resulted in the values shown in Table VI for the external convection coefficients on the side rails as a function of temperature.

TABLE VI
SIDE RAIL EXTERNAL CONVECTION COEFFICIENTS

T_h	100	500	800	1100	1400
h_o Btu/(hr-ft^2-°F)	87.0	63.1	53.6	47.1	41.1

If the carrier is not cooled internally, the internal air temperature will approximately equal the metal temperature of the side rails and convective heat transfer will be negligible. If the carrier is cooled internally, it is probable that air velocities due to forced convection will be rather low and that most of the heat transfer will be due to free convection induced by the high "g" field and large metal-to-air temperature differential. From the data on pages 1 and 2, section G504.2 of reference 2, the convection coefficient for the internal side of the side rail may be calculated at 31.1 Btu/(hr-ft^2-°F) if it is considered as a vertical flat plate and a metal-to-air temperature differential of 490 degrees Fahrenheit is estimated. This convection coefficient varies approximately as

the cube root of the temperature differential. Because the free convection inside the confined area of the carrier is likely to be a little less than that for a vertical flat plate in free air, an internal convection coefficient of 25 Btu/(hr-ft^2-°F) was assumed in this analysis.

From the above analysis, then, the side rail temperature at point (a) for any internal and external air temperatures may be calculated.

The side rail temperature at point (b) is strongly influenced by heat conduction from the bucket and its attachment structure, as well as by air temperatures and convection coefficients on the side rail surfaces. Temperature at this point is also influenced by conduction from the outer seal in the double seal arrangement shown in Figure 4. The effect of heat conduction to the side plate and tang can be ignored, since the critical stress point will normally be somewhat removed from the side plate and tang to an area where the temperature is nearly at a maximum.

A general expression for the temperature at point (b) may be written as follows:

$$T_b = T_{TB} - \eta_{c1} (T_{TB} - T_h) - \eta_{c2} (T_{TB} - T_c)$$

where

T_b = side rail temperature at point (b)

T_{TB} = bucket relative total temperature

T_h = air temperature on external side of side rail

T_c = air temperature on internal side of side rail

and η_{c1} and η_{c2} represent the cooling effectiveness, respectively, for the external air and the internal cooling air.

Values of η_{c1} and η_{c2} can be computed from the geometry and convection coefficients, and once they are known, T_b can easily be determined by use of the above equation.

We may assume an equivalent thermal circuit for computing T_b, as shown in Figure 11, which shows a cross section of the bucket carrier in the vicinity of point (b). The conductances X_1 and X_2 are as shown in Table V if the forward side of the carrier is considered. These would be replaced by X_3 and X_4, respectively, for the aft edge of the carrier. The conductance X_5 is through the side rail between point (b) and the internal cooling air. Similar X_6 is the conductance between point (b) and the air external to the carrier. If a seal is attached

to the carrier at point (b), then the conductances X_7 and X_8 must be included between point (b) and the side rail external air and between point (b) and the hot turbine gas.

The side rail and seal may be analyzed on the basis of one-dimensional thin fin theory. For a one-dimensional thin fin with boundary conditions as shown in Figure 12, the conductances between the base and the two air masses are given by

$$X_{b-o} = \frac{h_o}{a} \tanh as$$

$$X_{b-i} = \frac{h_i}{a} \tanh as$$

where

$$a = \sqrt{\frac{h_o + h_i}{12\ k\ t}}$$

In this case, s is generally sufficiently large so that

$$\tanh as \approx 1$$

and it will be assumed that

$$\tanh as = 1$$

The conductances X_5, X_6, X_7, and X_8 may then easily be calculated from the above equations. In this analysis, the convection coefficient on the lower side of the seal was assumed to be the same as for h_o, as shown in Table VI. On the upper side of the seal, a convection coefficient of 50 Btu/(hr-ft^2-°F) was assumed. The side rail and seal was assumed to be 0.015 inch in thickness and to have a thermal conductivity of 10.4 Btu/(hr-ft-°F).

If Figure 11 is again referenced and if the net heat flow into point (b) is equated to zero, then

$$(T_{TB} - T_b)(X_1 + X_8) + (T_c - T_b)(X_2 + X_5) + (T_h - T_b)(X_6 + X_7) = 0$$

or on rearranging,

$$T_b = T_{TB} - \frac{(X_6 + X_7)(T_{TB} - T_h) + (X_2 + X_5)(T_{TB} - T_c)}{X_1 + X_2 + X_5 + X_6 + X_7 + X_8}$$

Comparison of this equation with the previous equation for T_b shows

$$\eta_{c1} = \frac{X_6 + X_7}{X_1 + X_2 + X_5 + X_6 + X_7 + X_8}$$

$$\eta_{c2} = \frac{X_2 + X_5}{X_1 + X_2 + X_5 + X_6 + X_7 + X_8}$$

Values for η_{c1} and η_{c2} were computed for the forward side of the carrier as a function of the external air temperature, T_h, and are shown in Figures 13 and 14. Figure 13 is for the case of no internal cooling of the carrier side rail, $h_i = 0$, and Figure 14 is for the case where $h_i = 25$ Btu/(hr-ft^2-°F). For each of these cases, the four combinations of bucket internal cooling and heat shielding shown in Table V were also used. Configuration 1 included shielding but uncooled bucket airfoils. Configuration 2 included shielding and cooled bucket airfoils. Configuration 3 had no shielding and uncooled bucket airfoils. Configuration 4 had no shielding but cooled bucket airfoils.

TANG AND SIDE PLATE TEMPERATURES

A heat transfer analysis was also made of the tang and side plate region of the bucket carrier. Two cases were run on the same general heat transfer analysis computer program that was used for the bucket attachment heat transfer analysis. In the first case, a completely uncooled bucket and carrier assembly was used for the analysis; in the second case, a carrier cooled externally only, with the double seal arrangement, plus heat shielding over the bucket attachment areas. The external cooling air temperature, T_h, was assumed to be 720 degrees Fahrenheit. For both cases, the bucket relative temperature was assumed to be 1120 degrees Fahrenheit and the fan blade relative temperature to be 132 degrees Fahrenheit; these temperatures correspond to a fan inlet temperature of approximately 60 degrees Fahrenheit. The geometry for this analysis is as shown in Figure 8. It was also assumed that the fan blade tip tang was made of titanium.

For the uncooled case, the temperature of the side plate at point (d), shown in Figure 10, was 895 degrees Fahrenheit. At a corresponding point on the edge of the tang hole, the temperature was 855 degrees Fahrenheit. Based on the fan inlet temperature, the cooling effectiveness at these points can be calculated as follows:

$$\eta_{c_{plate}} = \frac{1120 - 895}{1120 - 60} = 0.217$$

$$\eta_{c_{tang}} = \frac{1120 - 855}{1120 - 60} = 0.250$$

PAYOFF FROM COOLING AND INSULATING

SINGLE-WALL VERSUS DOUBLE-WALL DUCTING

A study was undertaken to make a weight comparison of conventional single-wall ducting and the double-wall sandwich-type ducting previously described. The single-wall ducting requires an external insulation blanket in order to limit the heat rejection rate and external skin temperatures, and the weight of this insulation blanket should be included in any weight comparison. For double-wall ducting, it is possible to place all the insulation between the external structural wall and the internal heat shield. Alternatively, some of the insulation could be placed inside and some outside the structural wall. This would reduce problems of thermal expansion between the two duct walls and yield a slightly smaller structural wall diameter, but would increase the need for bellows between adjacent sections of ducting. For this study, the choice was made to place all the insulation between the internal and external walls of the double-wall ducting.

To estimate the amount of insulation required by any duct design, it was decided to limit the heat rejection rate from the duct surface to 922 Btu/(hr-ft^2) with an external skin temperature of 337 degrees Fahrenheit. These figures are consistent with the ducting figures for a previous cruise fan design, and assume some compartment cooling by forced convection. The characteristics of the assumed insulation are shown in Figure 15.

The required wall thickness for the single-wall duct was based on the design stress versus temperature curve shown in Figure 16 for Rene' 41. The design stress was assumed to be twice the hoop stress computed from the internal pressure in order to allow for other unknown external loads. The metal temperature was assumed to be equal to the internal gas temperature, since the internal convection coefficient is quite large compared to the conductance of the insulation blanket.

It was also necessary to assume a minimum wall thickness. Based on past experience with ducting, it was decided that a minimum thickness of 0.015 inch would be adequate for simple ducting but that a minimum of 0.025 inch would be required in more complicated ducting with multiple loads, such as diverter valves and scrolls. Structural walls of both the single-wall and double-wall ducts were based on these minimum thicknesses, and the weight comparison was made for both values.

For the double-wall ducting, it was assumed that the liner would be 0.010-inch material for all designs. Also, the total weight of the two walls was increased by 10 percent to allow for convolutions and attachments between the walls. It was felt that the two conceptual double-wall duct designs would not differ greatly in weight.

The results of this weight study are shown in Figures 17 and 18. Figure 17 is for a minimum structural wall thickness of 0.015 inch; it shows duct weight in pounds per square foot of surface area versus gas temperature. The weight of single-wall ducting is also a function of the product of internal pressure times diameter, denoted by "PD" on these curves. The weight of double-wall ducting is independent of PD for values under 1000 pounds per inch, since the stress never exceeds the allowable stress with a 0.015-inch wall. Figure 18 is similar to Figure 17 except that it is for a minimum structural wall thickness of 0.025 inch. An upper limit of 1500 degrees Fahrenheit has been assumed for the Rene' 41 single-wall duct because of its low resistance to oxidation above this temperature.

Figure 19 shows the gas temperatures at which the single-wall and double-wall ducts have equal weight versus the product of internal pressure times diameter, PD. Also shown on this figure is the temperature - versus - PD region covered by the core engine cycles given in Table II. Duct diameters are based on a flow Mach number of 0.3. This shows that all core engine cycles except cycles A and B would have lighter ducts if they were of double-wall design. However, in locations where multiple ducts are required, such as in a cruise fan nacelle, cycles C, D, and E could still be lighter if the single-wall ducting were used.

The cool outer wall of the double-wall ducting may also have other advantages. With a surface temperature of only 337 degrees Fahrenheit, much greater latitude in selection of materials is possible. Since the outer wall and inner wall would not be welded or brazed together, there is no problem in choosing different materials for these two parts. Thermal expansion of the outer wall could be greatly reduced, and the number and size of bellows between sections of duct could be reduced significantly.

BUCKET-CARRIER COOLING

After devising means of cooling buckets and carriers and of estimating temperatures at various critical locations, it becomes desirable to make a comparative weight study of the various means of cooling. With the basic geometry shown in Figure 8 as the base point, carrier weights for a number of cooling schemes and bucket relative temperatures were calculated. The results of this study are shown in Figure 20, which shows the relative carrier weight versus bucket relative temperature for an uncooled design and for six cooled designs.

In Figure 20, curve 1 is for a completely uncooled design. This design has no heat shielding over the attachment area and no double seal arrangement. Hot turbine gas is in direct contact with the exterior of the carrier side rails and side plates.

Curve 2 is for a carrier with the double seal arrangement, both fore and aft, but with no heat shield to protect the attachment area. Cool air of 110 degrees Fahrenheit flows between the inner and outer seals and cools the bucket side rails and side plates. There is no internal cooling of buckets or carrier.

Curve 3 is similar to curve 2 except that the cooling air has been assumed to be at a temperature midway between the bucket relative temperature and 110 degrees Fahrenheit.

Curve 4 is similar to curve 3 except that shielding has been added to protect the bucket attachment area.

Curve 5 is for a carrier with the forward side cooled as for curve 4, but with the aft side cooled by 110-degree-Fahrenheit cooling air. The carrier and bucket are also cooled internally with 110-degree-Fahrenheit cooling air. A heat shield covers only the forward side of the bucket attachment area. This cooling scheme would be similar to that shown in Figure 4.

Curve 6 is similar to curve 5 except that there is no double seal on the forward side, and hot turbine gas is in direct contact with the forward side rail.

Curve 7 is for a carrier which is cooled internally only. Buckets are uncooled, and hot gas is in direct contact with the exterior of the carrier side rails and side plates. The attachment area is shielded on both sides, but there is no second seal at the outer radius of the carrier. Cooling air at 140 degrees Fahrenheit enters the carrier as shown in Figure 6.

The method of calculating weights for the bucket carriers is described in Appendix II. The method of inducing cooling air into the carrier by scoops at the fan tip, as shown in Figure 5, was not evaluated, since it would appear to be much too heavy by comparison to the above schemes.

ADVANCED MATERIALS AND TEST PROGRAMS

A brief look was given to to sheet materials for use as hot duct liners in the 1500-degree-Fahrenheit to 1800-degree-Fahrenheit temperature range. The selection of materials is complicated by the relatively long design life required in cruise fan applications. Although the duct liners may not be heavily loaded, it is doubtful that any of the presently available materials will satisfy design life requirements on the order of 10,000 hours from an oxidation and erosion loss standpoint. Although data on long life oxidation resistance is very meager, the following materials appear to offer the best combination of properties for this application.

TABLE VII
POSSIBLE LINER MATERIALS

Alloy	Class	Major Drawback
Hastelloy X	Ni Base	Stress Rupture Life
L605 or X-45	Co Base	Embrittlement
TD-Ni-Cr	Ni Base	Availability
Rene' Y	Ni Base	Availability

Several possible approaches to the solution of the long-term oxidation problem may be taken and should be considered in planning future work in materials development and component tests. First, it may be possible to develop combinations of liner thicknesses and materials which would have a long oxidation life. Development of these liners would require long time tests under dynamic conditions.

A second approach could be to design the liners for a shorter life but design the ducting in such a way that either the liners or the complete duct could be replaced relatively easily and cheaply at regular intervals. This approach would require testing to establish more accurately the design life of various liner materials.

A third approach could be to develop oxidation-resistant coatings for the liners. Again, this approach would require long time tests of ducts under dynamic conditions.

If the turbine carrier cooling scheme shown in Figure 6 is used, some deterioration in fan tip performance is very likely to occur because of the low velocity air flowing into the fan stream on the suction side of the blade tip. A test program to evaluate the cooling effectiveness of this scheme and its effect on fan aerodynamic performance could be a relatively inexpensive addition to some future fan test. This testing could also investigate means of minimizing fan performance loss by proper location and direction of the cooling air holes.

Another desirable addition to future fan component tests would be the substantiation of the convection coefficients estimated for the bucket carrier, both internally and externally. Accurate calculation of these convection coefficients is difficult because of the complicated geometry and leakage flow paths.

CONCLUSIONS

1. Sandwich-type duct construction is superior in terms of weight for all gas temperatures above about 1500 degrees Fahrenheit. For ducts with high internal pressures and large diameters, sandwich-type construction may be superior above temperatures of about 1200 degrees Fahrenheit.

2. The low external wall temperatures of sandwich-type ducting may have advantages which offset the additional complexity of double-wall construction.

3. Turbine bucket airfoils probably do not require cooling for relative gas temperatures up to about 1400 degrees Fahrenheit. No payoff can be shown. Only one core engine cycle envisioned is likely to exceed a 1400-degree-Fahrenheit relative gas temperature.

4. Bucket-carrier and tip-tang cooling is required for bucket relative temperatures of about 1200 degrees Fahrenheit and may be advantageous at about 1100 degrees Fahrenheit. Most planned core engines will produce bucket relative temperatures of 1100 degrees Fahrenheit or higher; many, above 1200 degrees Fahrenheit.

5. Any system of bucket-carrier cooling must add a minimum of weight to the carrier if it is to pay off.

BIBLIOGRAPHY

1. Cooper, A. L., Nomogram Application to Heat Transfer Analysis in Gas-Turbine Rotor System, General Electric Technical Information Series Report No. R56SE66, Lynn, Massachusetts, 1956.

2. Heat Transfer and Fluid Flow Design Data, General Electric General Engineering Laboratory, Schenectady, New York, 1963.

3. Stemens, G. L., and Campbell, D. J., Program THTB for Analysis of General Transient Heat Transfer Systems, General Electric Technical Information Series Report No. R60FPD647, Evendale, Ohio, 1961.

4. Asmus, F.J., Parametric and Preliminary Design Studies of High-Speed and Low-Speed Cruise Fan Propulsion Systems, U.S. Army Aviation Materiel Laboratories Technical Report 65-57, March 1966.

DISTRIBUTION

US Army Materiel Command	5
US Army Mobility Command	5
US Army Aviation Materiel Command	4
US Army Forces Southern Command	1
Chief of R&D, DA	1
US Army Aviation Materiel Laboratories	15
US Army R&D Group (Europe)	2
US Army Test and Evaluation Command	1
US Army Combat Developments Command, Fort Belvoir	2
US Army Combat Developments Command Transportation Agency	1
US Army Aviation School	1
US Army Infantry Center	2
US Army Tank-Automotive Center	2
US Army Aviation Test Board	3
US Army Aviation Test Activity	2
Air Force Flight Test Center, Edwards AFB	1
US Army Field Office, AFSC, Andrews AFB	1
Air Force Aeropropulsion Laboratory	1
Systems Engineering Group (RTD), Wright-Patterson AFB	3
Systems Engineering Group (AFSC), Wright-Patterson AFB	1
Naval Air Systems Command, DN	2
Bureau of Naval Weapons, DN	4
Chief of Naval Research	2
US Naval Air Station, Norfolk	1
Commandant of the Marine Corps	1
Marine Corps Liaison Officer, US Army Transportation School	1
Ames Research Center, NASA	1
Lewis Research Center, NASA	1
NASA Representative, Scientific and Technical Information Facility	2
NAFEC Library (FAA)	2
US Army Board for Aviation Accident Research	1
Bureau of Safety, Civil Aeronautics Board	2
US Naval Aviation Safety Center, Norfolk	1
Federal Aviation Agency, Washington, D. C.	1
Defense Documentation Center	20
US Government Printing Office	1

APPENDIX I
TURBINE BUCKET RELATIVE TEMPERATURE

In a turbine, the total gas temperature relative to the bucket is substantially less than the turbine inlet gas total temperature; this is because of the velocity of the bucket relative to the absolute gas velocity. The ratio between the bucket relative temperature and the turbine inlet temperature is a function of the turbine vector diagram and can be calculated as follows. If the vector diagram in Figure 21 is referenced, it can be seen that the bucket relative temperature can be calculated as follows:

$$T'_{TB} = T'_{5.4} - \frac{1}{2gJc_p}\left[V_1^2 - V_{a_1}^2 - (V_{u_1} - U)^2\right] =$$

$$T'_{5.4} + \frac{1}{2gJc_p}\left(U^2 - 2\,V_{u_1}\,U\right) =$$

$$T'_{5.4} - \frac{V_{u_1}^2}{2gJc_p}\left(2\,\frac{U}{V_{u_1}} - \frac{U^2}{V_{u_1}^2}\right)$$

Also, the nozzle tangential velocity can be calculated from

$$V_{u_1}^2 = 2gJc_p\,\eta_N\,T_{5.4}\left[1 - (P_{S5.5}/P_{5.4})^{\frac{\gamma-1}{\gamma}}\right](\cos^2\alpha)$$

Substitution of this relation into the previous equation and dividing by $T_{5.4}$ gives

$$T'_{TB}/T'_{5.4} = 1 - \left[1 - (P_{S5.5}/P_{5.4})^{\frac{\gamma-1}{\gamma}}\right](\eta_N \cos^2\alpha)\left(2\,\frac{U}{V_{u_1}} - \frac{U^2}{V_{u_1}^2}\right)$$

If, for typical values, it is assumed that

$\eta_N = 0.97$
$\gamma = 4/3$
$\alpha = 20$ degrees,

then $T_{TB}/T_{5.4}$ may be plotted versus the turbine pressure ratio for various values of the velocity ratio, U/V_{u_1}, as shown in Figure 1. The velocity ratio will normally be between 0.4 and 0.5 for most tip-turbine designs.

APPENDIX II
CALCULATION OF BUCKET-CARRIER WEIGHT

Variation of bucket-carrier weight with bucket relative temperature and method of cooling were estimated by starting with the basic geometry of Figure 8 and by varying the weight of various components according to their temperatures and loads. The basic carrier design of Figure 8 had its total weight distributed among its components as shown in Table VIII.

TABLE VIII
WEIGHT DISTRIBUTION FOR BASIC CARRIER DESIGN

Component	Weight (Pounds)
Buckets (including box and tip shroud)	.437
Side Rails	.142
Side Plate	.558
Seal	.356
Tang	.434
Total	1.927

This basic design was uncooled and designed for a bucket relative temperature of 1000 degrees Fahrenheit.

The method by which these component weights were adjusted for variations in temperature can best be shown by an example. Consider the variation in weight of this uncooled design as the bucket relative temperature varies. The weight of the buckets, tip shroud, and attachment box has been considered to be independent of temperature in this study, since their weight is based on minimum stock thickness considerations rather than stress limits. However, an upper limit of 1400 degrees Fahrenheit metal temperature was placed on these parts. Also, the weight of the inner seal was considered to be independent of bucket relative temperature, since its metal temperature was always low enough for its limiting stress to be essentially constant.

The carrier side rails are designed to their stress limit, which is directly influenced by metal temperature. For this analysis, Rene' 41 material was assumed for the side rails and side plates, with the design stress versus temperature characteristics shown in Figure 22. The side rail must carry the load of the buckets and the seal, plus its own load. The side rail thickness is varied with its load and temperature so that its stress limit is not exceeded. It can be assumed that the stress at any point in the side rail is proportional to the total load and inversely proportional to the rail thickness. Since the weight of the side rail is proportional to the thickness, then

$$\sigma = K \left(\frac{W_B \quad W_S + W_R}{W_R}\right)$$

If it is assumed that for the uncooled design the side rail temperature is equal to the relative bucket temperature, then the allowable design stress at 1000 degrees Fahrenheit from Figure 22 is 88,000 pounds per square inch. With the above equation for the base case, then

$$88{,}000 = K \left(\frac{0.437 + 0.356 + 0.142}{0.142}\right)$$

If this equation is solved for K, then

$$K = 13{,}360 \text{ pounds per square inch}$$

Now that K is evaluated, the above equations may be solved for the side rail weight in terms of the bucket and seal weight and the allowable stress to get

$$W_R = \frac{K\ (W_B + W_S)}{\sigma_a - K}$$

or

$$W_R = \frac{10{,}590}{\sigma_a - 13{,}360} \text{ pounds}$$

The allowable design stress, σ_a, was determined from Figure 22 for each temperature and the corresponding side rail weight computed.

A similar analysis for the side plate gave the following equation for the side plate weight:

$$W_P = \frac{35{,}480\ (W_B + W_S + W_R)}{\sigma_a - 35{,}480}$$

The allowable stress for the side plate was evaluated at the temperature at point (d) in Figure 10. The temperature at this point for the uncooled design was calculated on the basis of

$$\eta_{c_{plate}} = 0.29$$

rather than on the basis of $\eta_{c_{plate}} = 0.217$, as shown on page 15. This change was made because test data on actual fans have indicated somewhat

higher values for $\eta_{c_{plate}}$. This discrepancy may be due in part to cool air leakage past the tang and into the interior of the carrier.

Another similar analysis gave the following equation for the weight of the titanium tip tang:

$$W_T = \frac{20{,}000\ (W_B + W_S + W_R + W_A)}{\sigma_a}$$

In this case, however, it was assumed that the tip tang carried the load of the buckets, seals, side rail, and side plate but not its own load. The tang temperature was calculated on the basis of

$$\eta_{c_{tang}} = 0.33$$

and the allowable design stress was as shown in Figure 23.

The following table summarizes the weight calculations for this case:

TABLE IX
WEIGHT CALCULATION SUMMARY FOR UNCOOLED CARRIER

T_{TB} (°F)	W_B (lb)	W_S (lb)	W_R (lb)	W_P (lb)	W_T (lb)	Total Weight (lb)	Relative Weight
900	.437	.356	.118	.543	.408	1.862	.966
1000	.437	.356	.142	.558	.434	1.927	1.000
1100	.437	.356	.180	.580	.502	2.055	1.066
1200	.437	.356	.339	.680	.980	2.792	1.449
1300	.437	.356	1.518	1.425	-	-	-

A similar approach was employed for calculating the weights of cooled bucket and carrier configurations. In configurations employing the double seal arrangement, the weight of the second seal was assumed to be equal to the first. If the carrier had the double seal arrangement on one side only, the increased weight was assumed to be only half of the first seal. For cooled configurations, the side rail temperatures were calculated at both points (a) and (b) in Figure 10. It was assumed that the rail could be made in two thicknesses: the outer 20 percent designed for the temperature at point (b) and the inner 80 percent designed for the temperature at Point (a).

In all the cooled configurations, the temperature of the side plate was sufficiently low that its allowable stress was independent of temperature. Tang temperatures for the cooled cases were estimated from the following equation:

$$T_{tang} = T_{TB} - 0.683\ (T_{TB} - T_h) - 0.15\ (T_{TB} - 110^{\circ}F)$$

except for case 7, where it was assumed that

$$\eta_{c_{tang}} = 0.4$$

The above relations were estimated from the results of the heat transfer analysis on the side plate and tang.

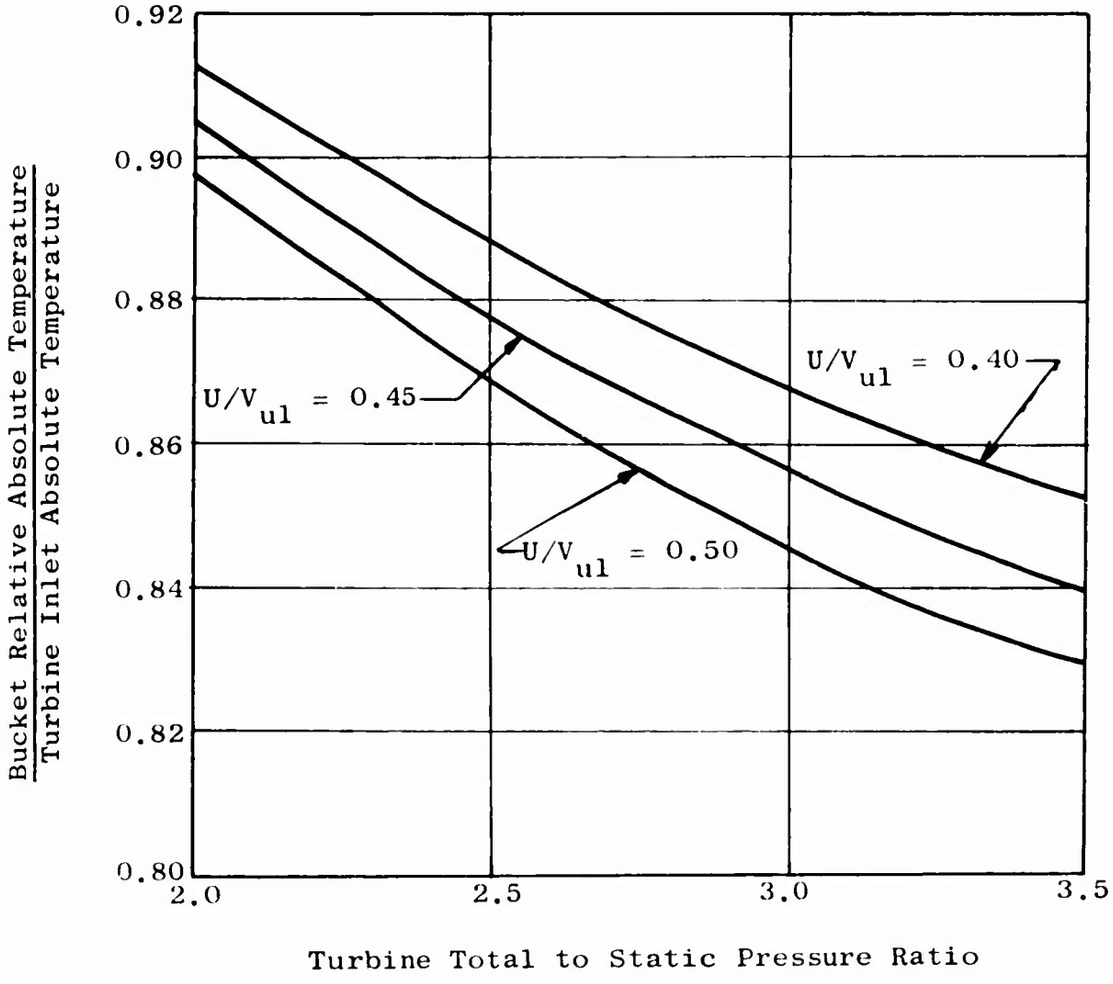

Figure 1. Turbine Bucket Relative Temperatures.

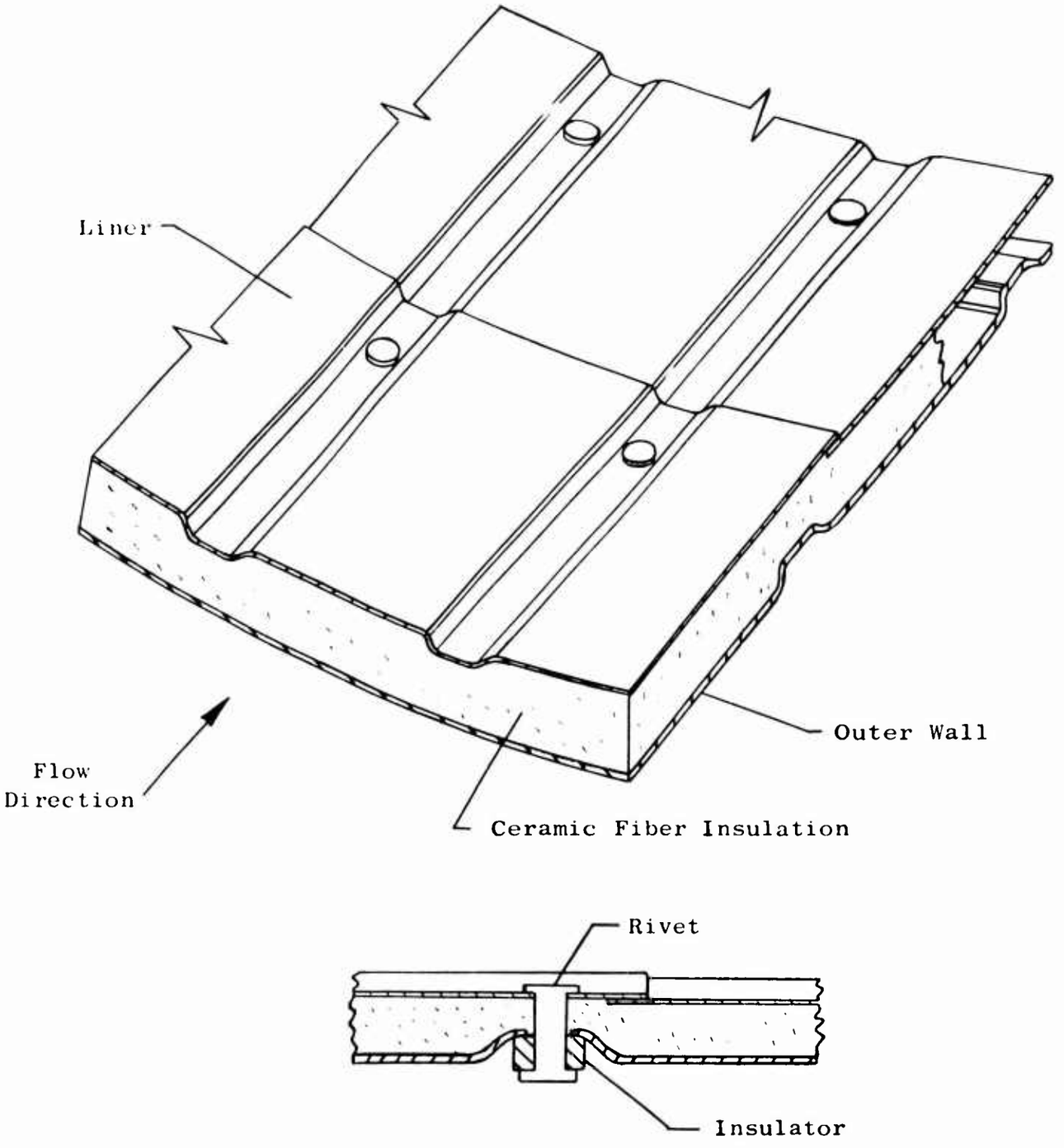

Figure 2. Double-Wall Duct Construction Section Showing Attachment Detail.

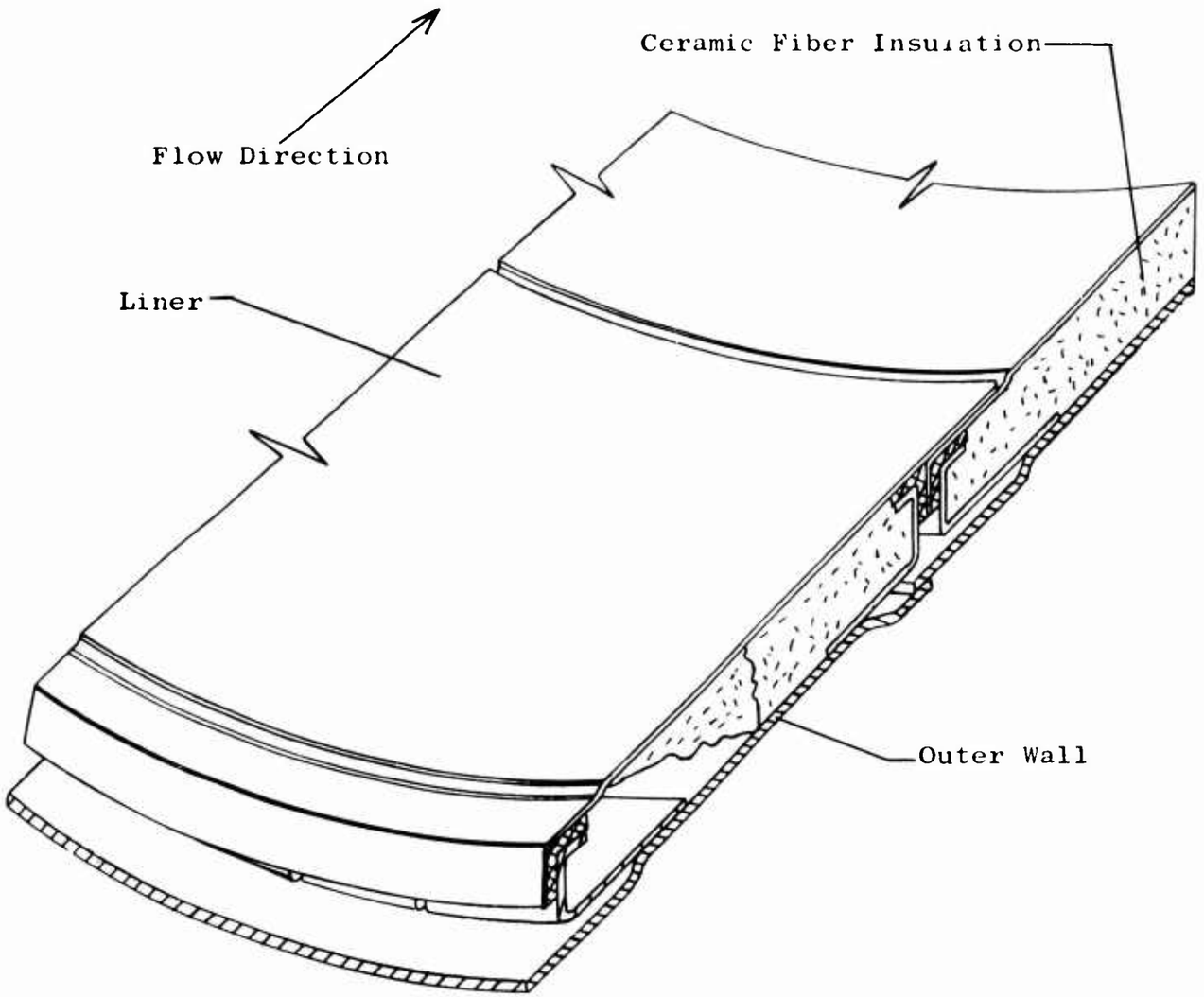

Figure 3. Alternate Double-Wall Duct Construction.

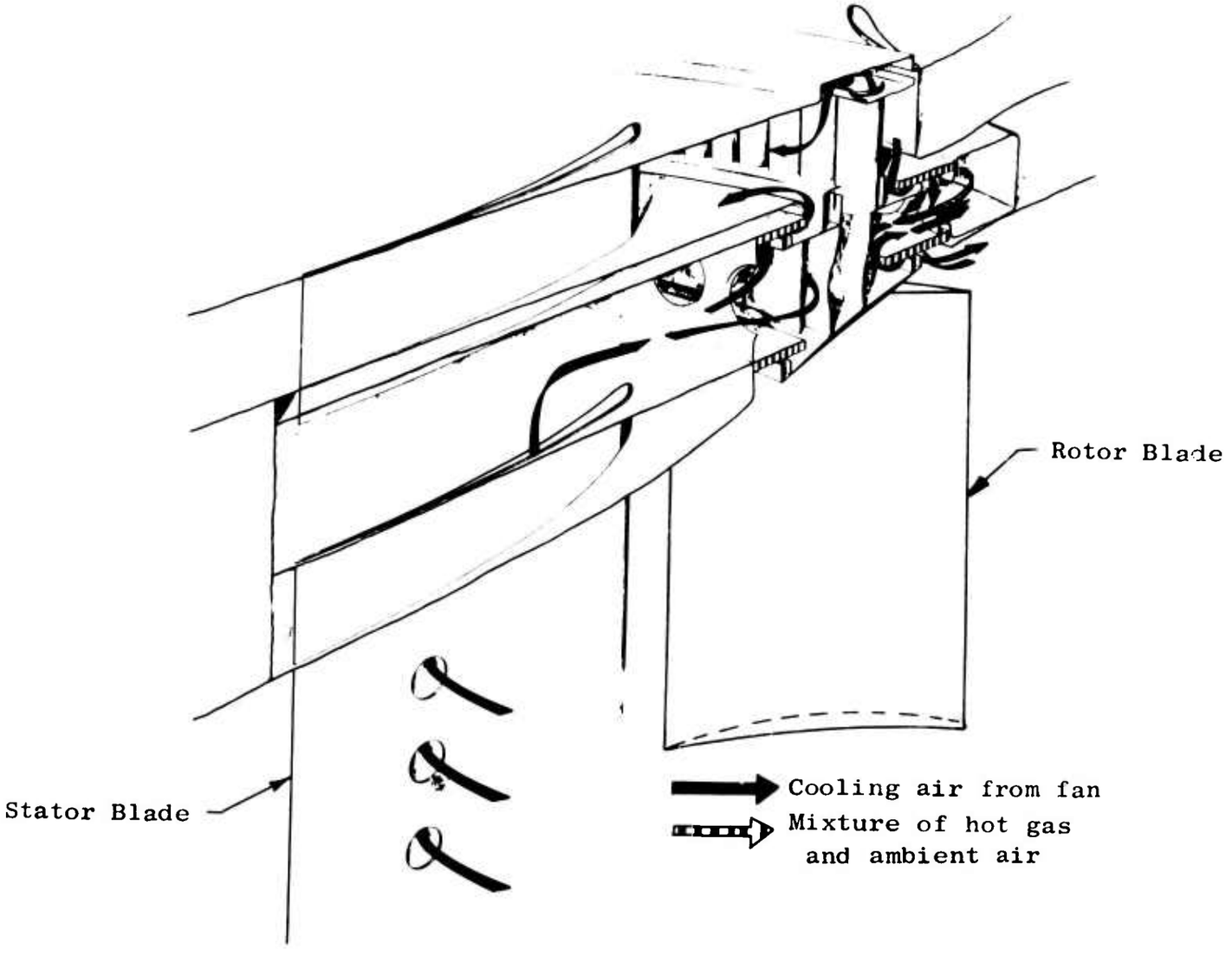

Figure 4. Tip-Turbine Cooling Scheme.

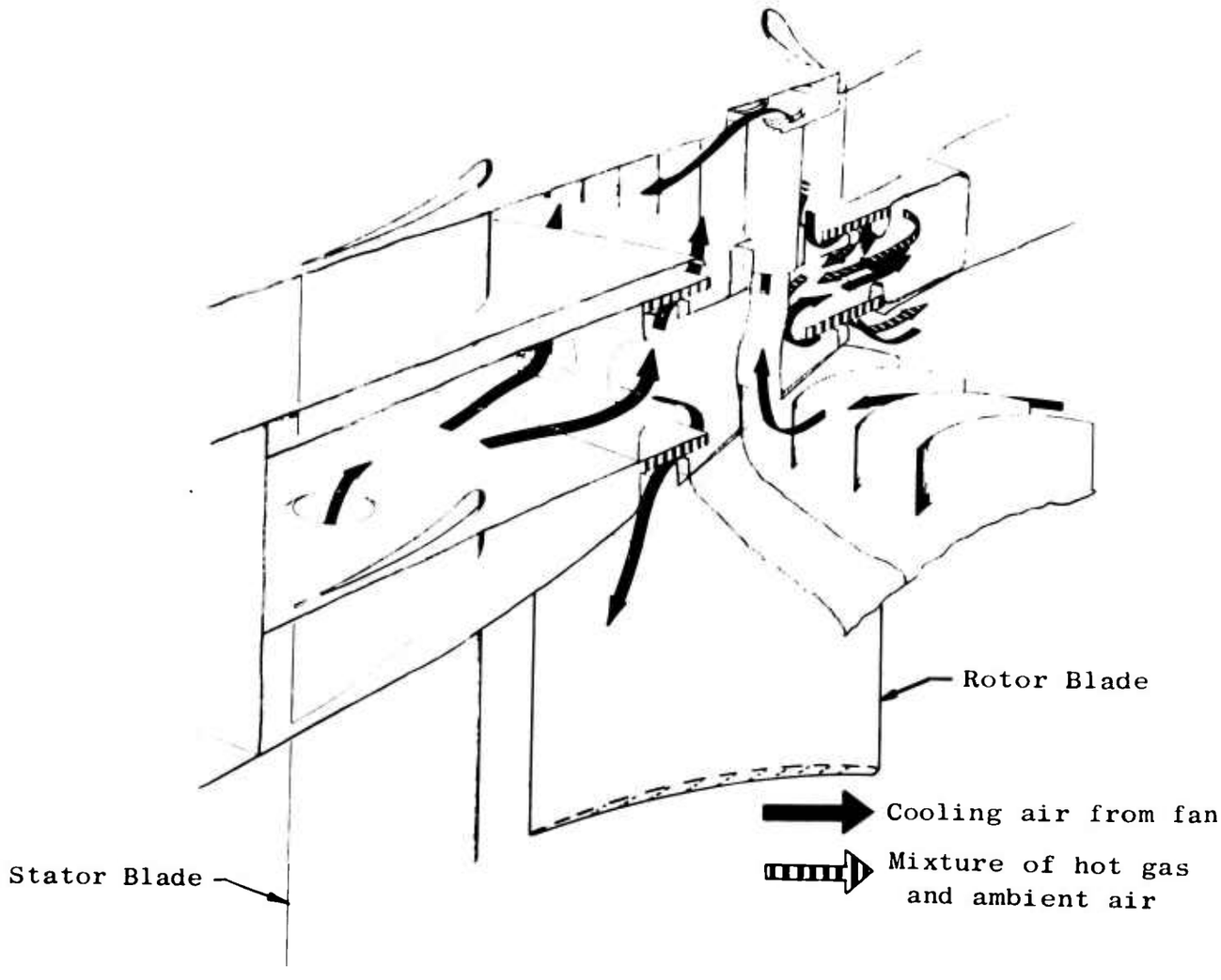

Figure 5. Alternate Bucket-Carrier Cooling Scheme.

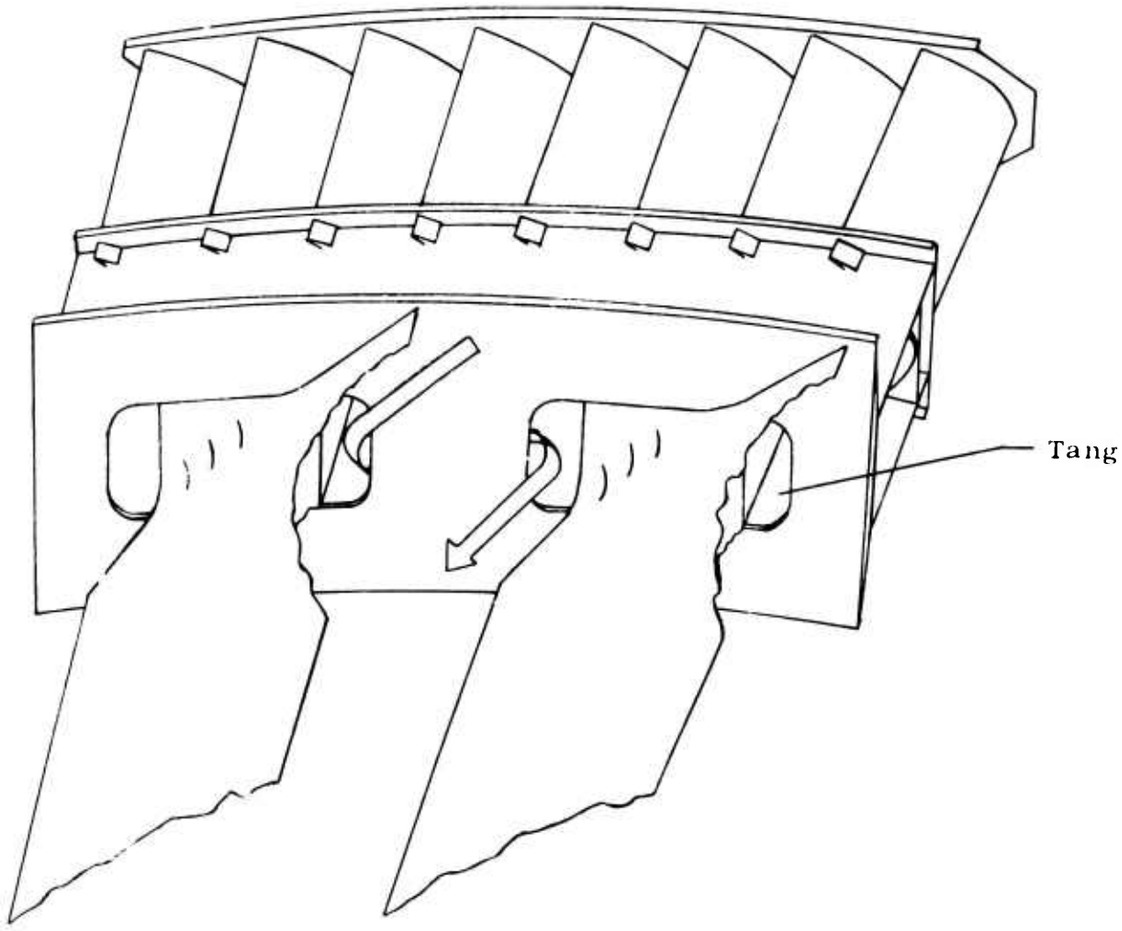

Figure 6. Internal Cooling of Carrier With Leakage Past Tip Tangs.

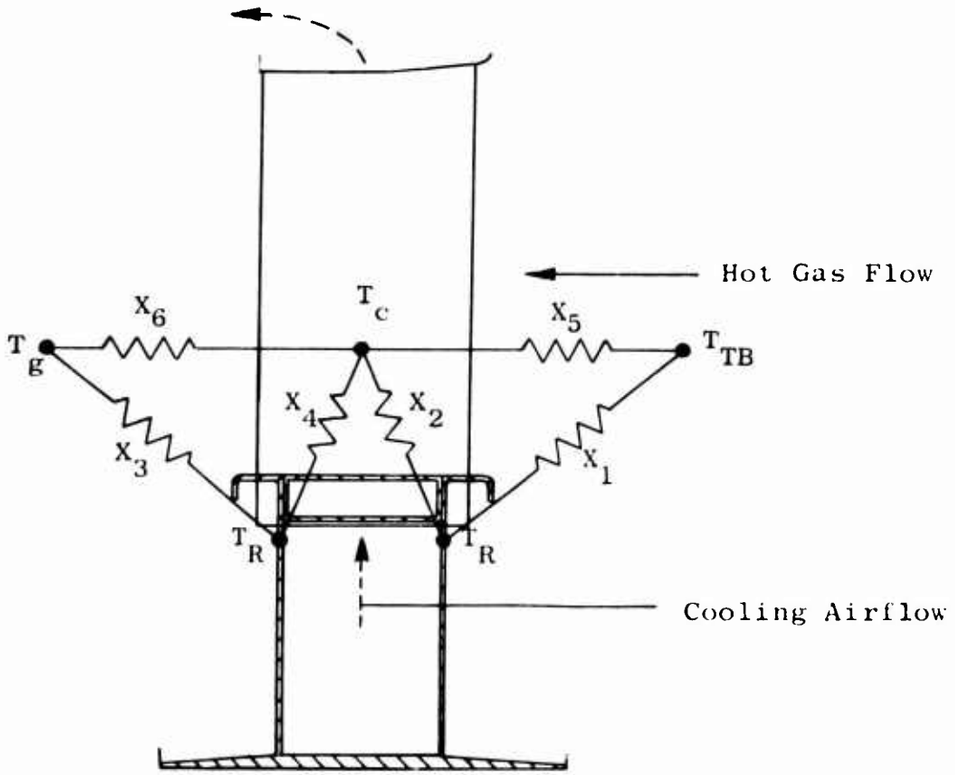

T_{TB} = hot gas temperature, degrees Fahrenheit

T_c = cooling air temperature, degrees Fahrenheit

T_{rail} = rail temperature at base of bucket attachment, degrees Fahrenheit

Figure 7. Equivalent Thermal Network for Bucket Attachment.

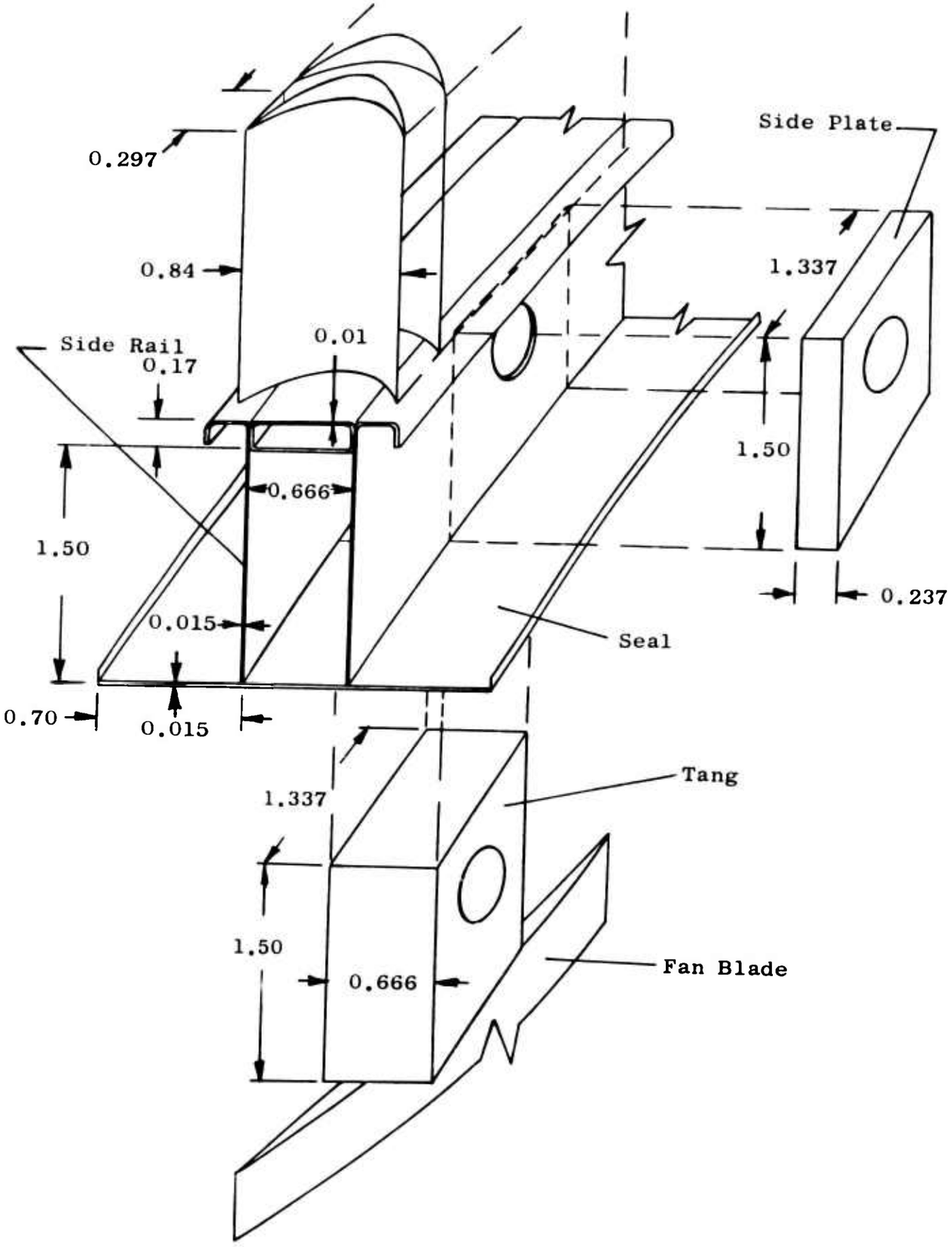

Figure 8. Assumed Carrier Geometry for Heat Transfer Analysis.

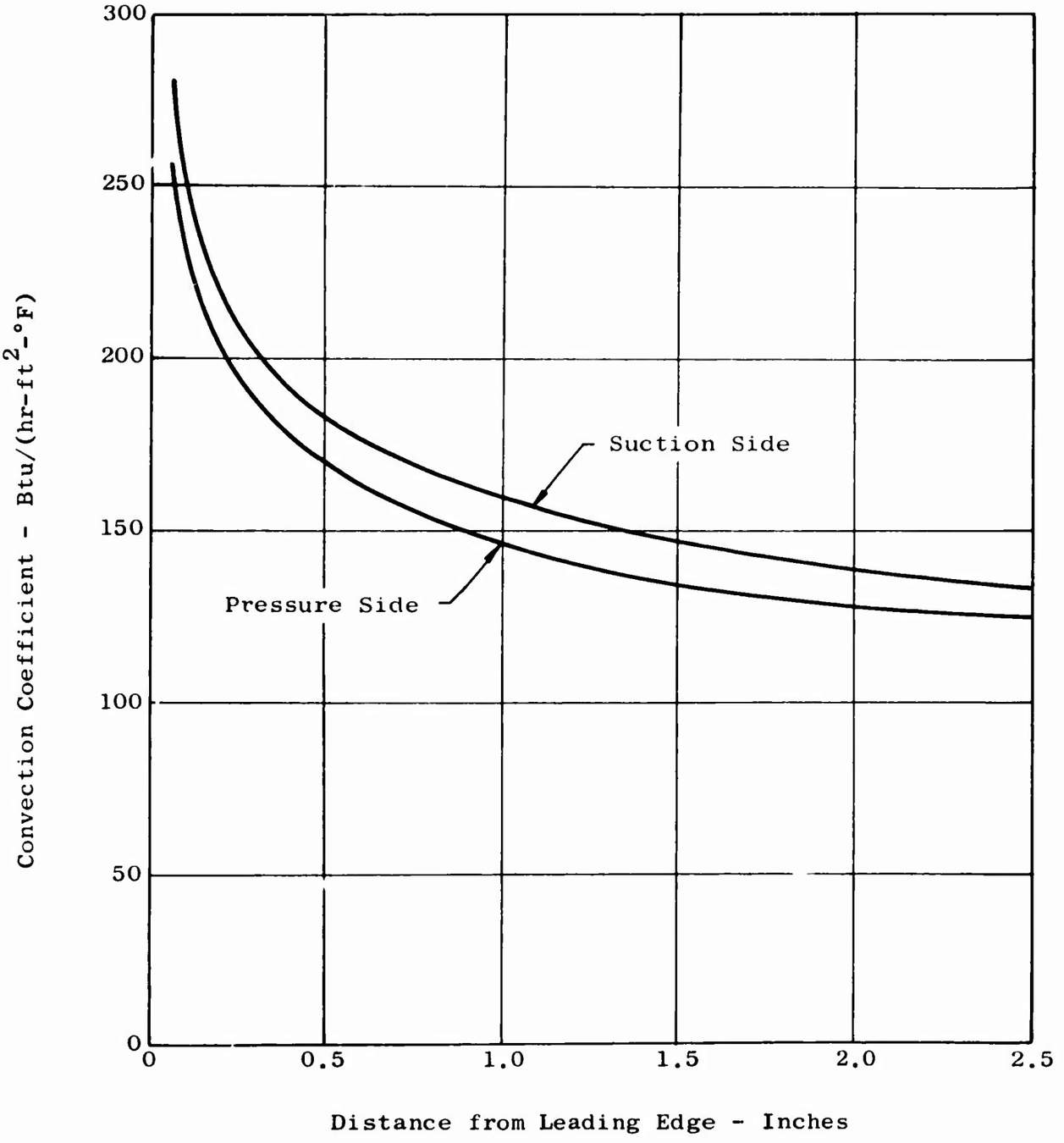

Figure 9. Bucket External Surface Convection Coefficient.

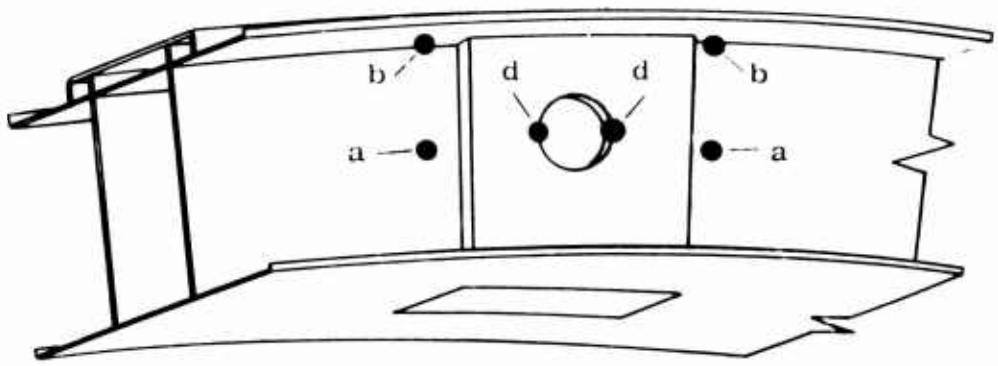

Carrier with Double Seals and Heat Shield

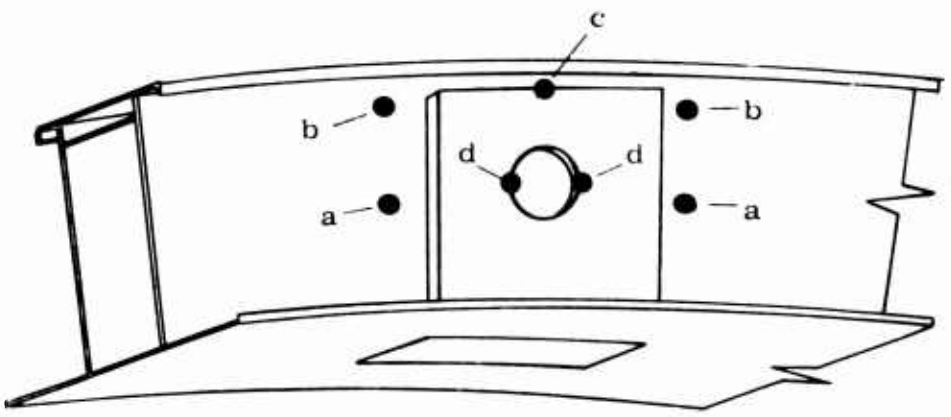

Carrier with Single Seal and No Heat Shield

● Indicates Point of Critical Stress

Figure 10. Location of Critical Stress Points on Carriers.

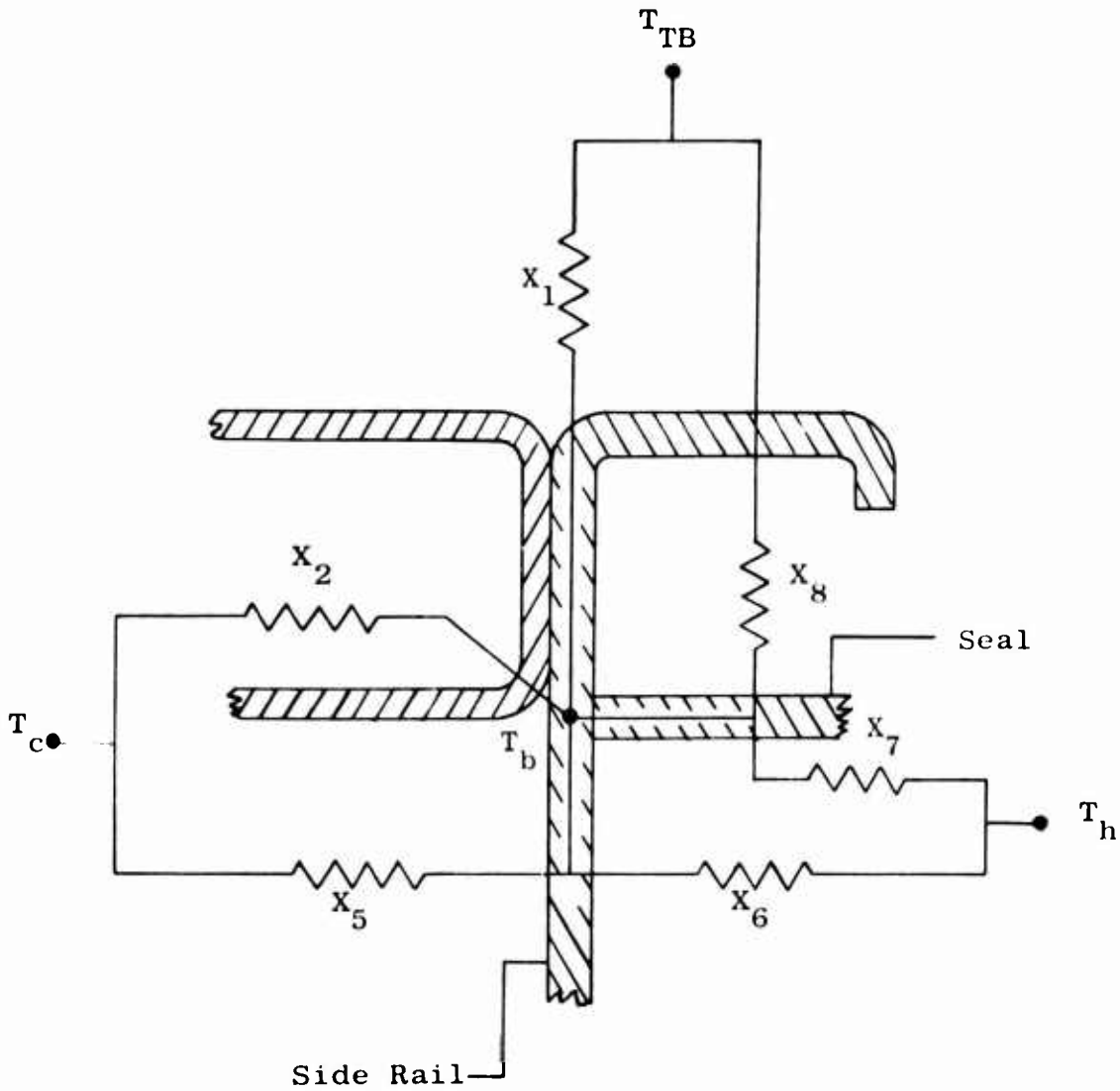

Figure 11. Equivalent Thermal Circuit for Computing Temperature at Point (b).

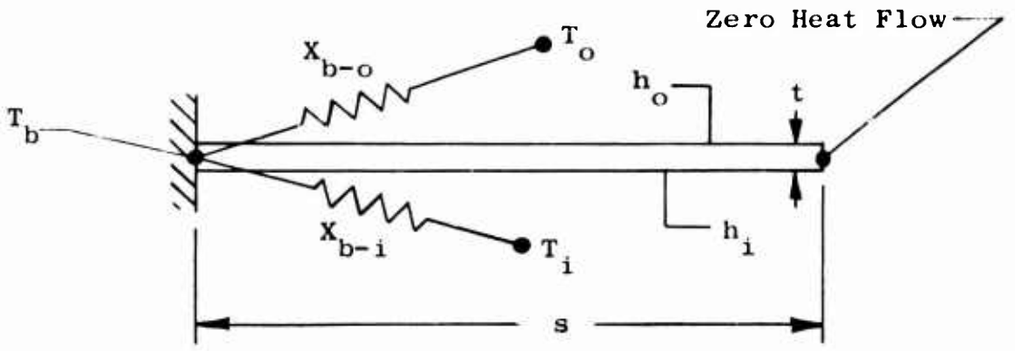

$$X_{b-o} = \left(h_o/a\right) \tanh as$$

$$X_{b-i} = \left(h_i/a\right) \tanh as$$

$$a = \sqrt{h_o + h_i/kt\,12}$$

k = thermal conductivity for fin

Figure 12. Equivalent Conductances of One-Dimensional Thin Fin.

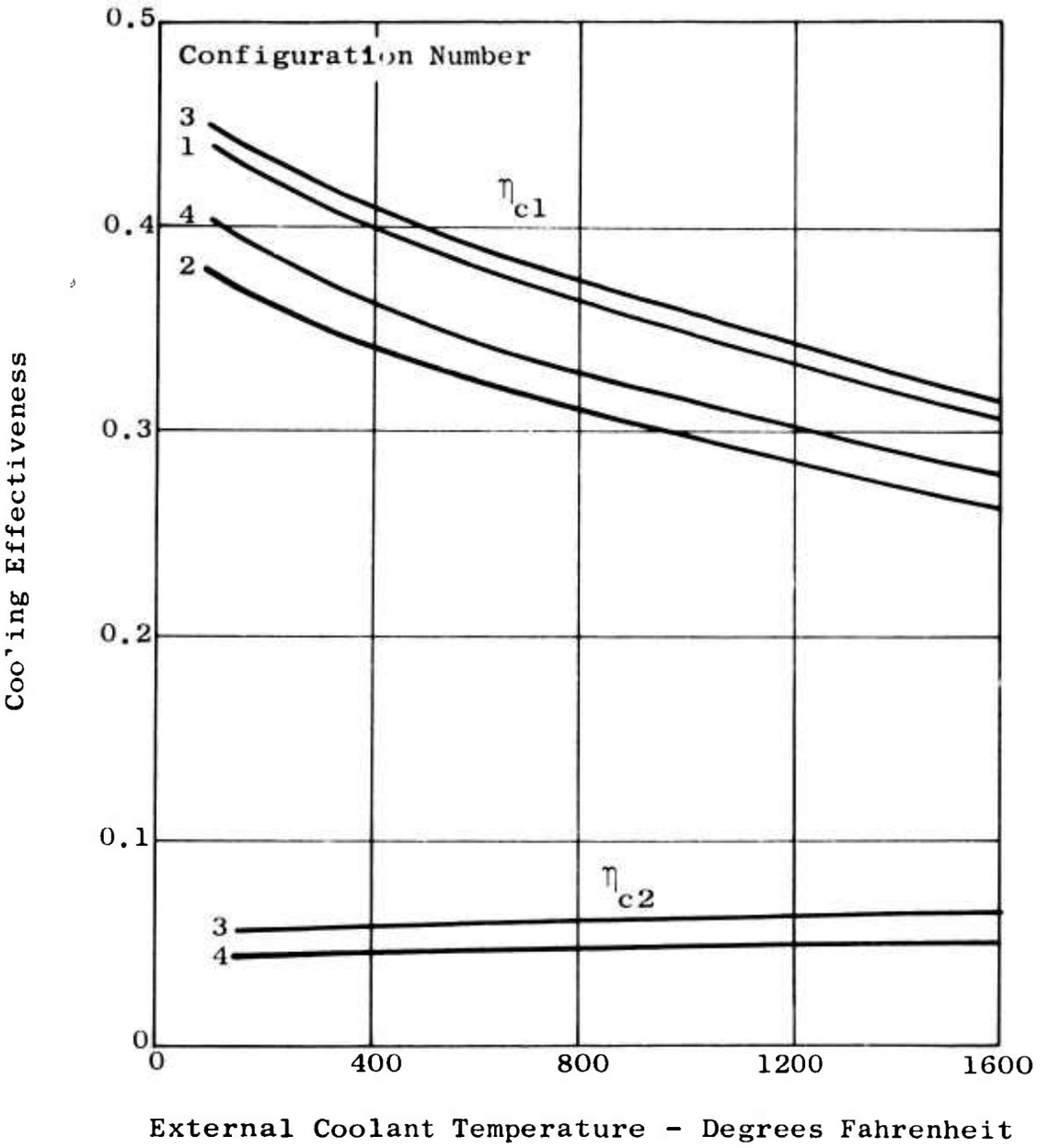

Figure 13. Cooling Effectiveness at Rail Outer Edge for an Internal Convection Coefficient of 0.

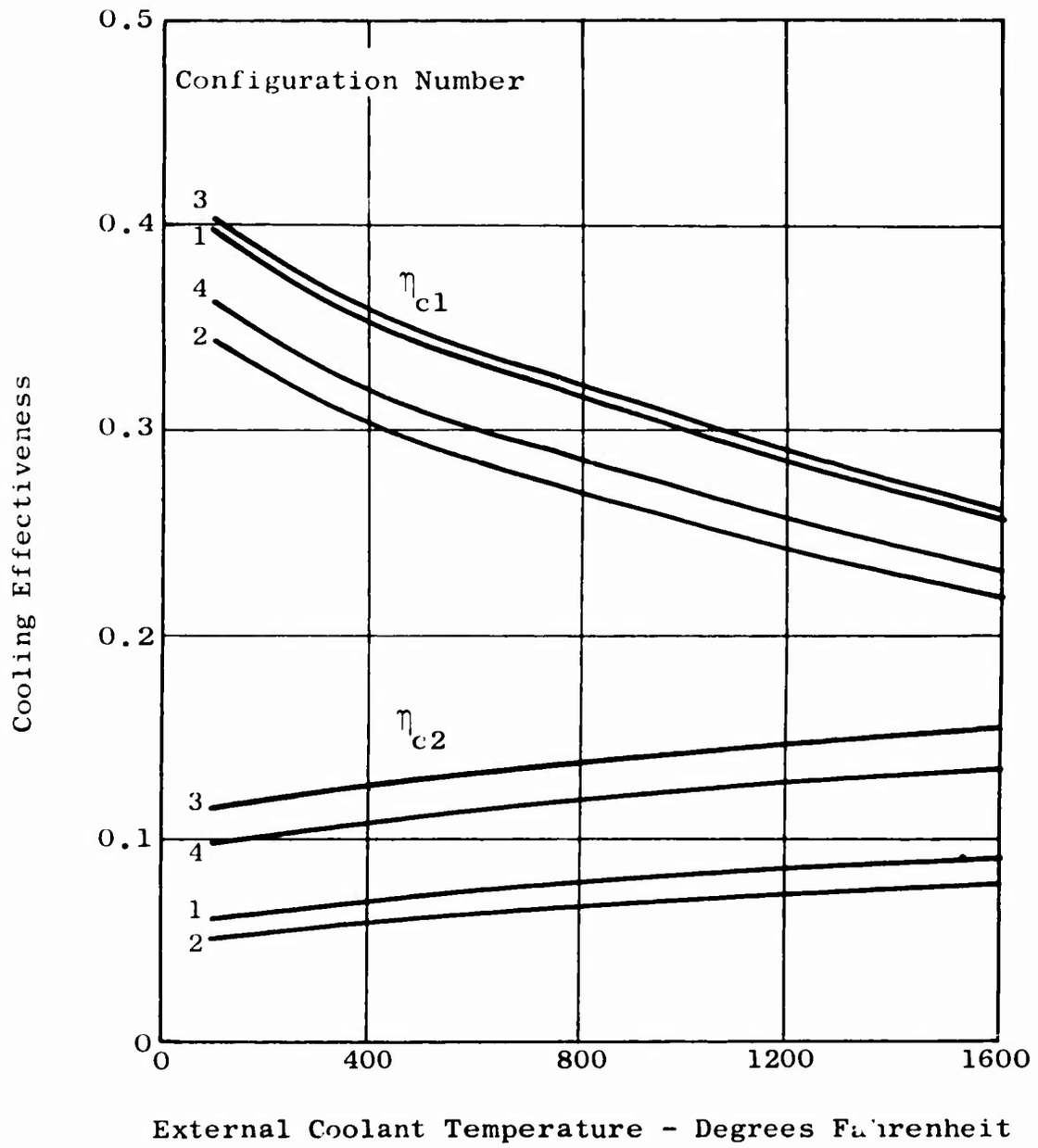

Figure 14. Cooling Effectiveness at Rail Outer Edge for an Internal Convection Coefficient of 25 Btu/(hr-ft^2-°F).

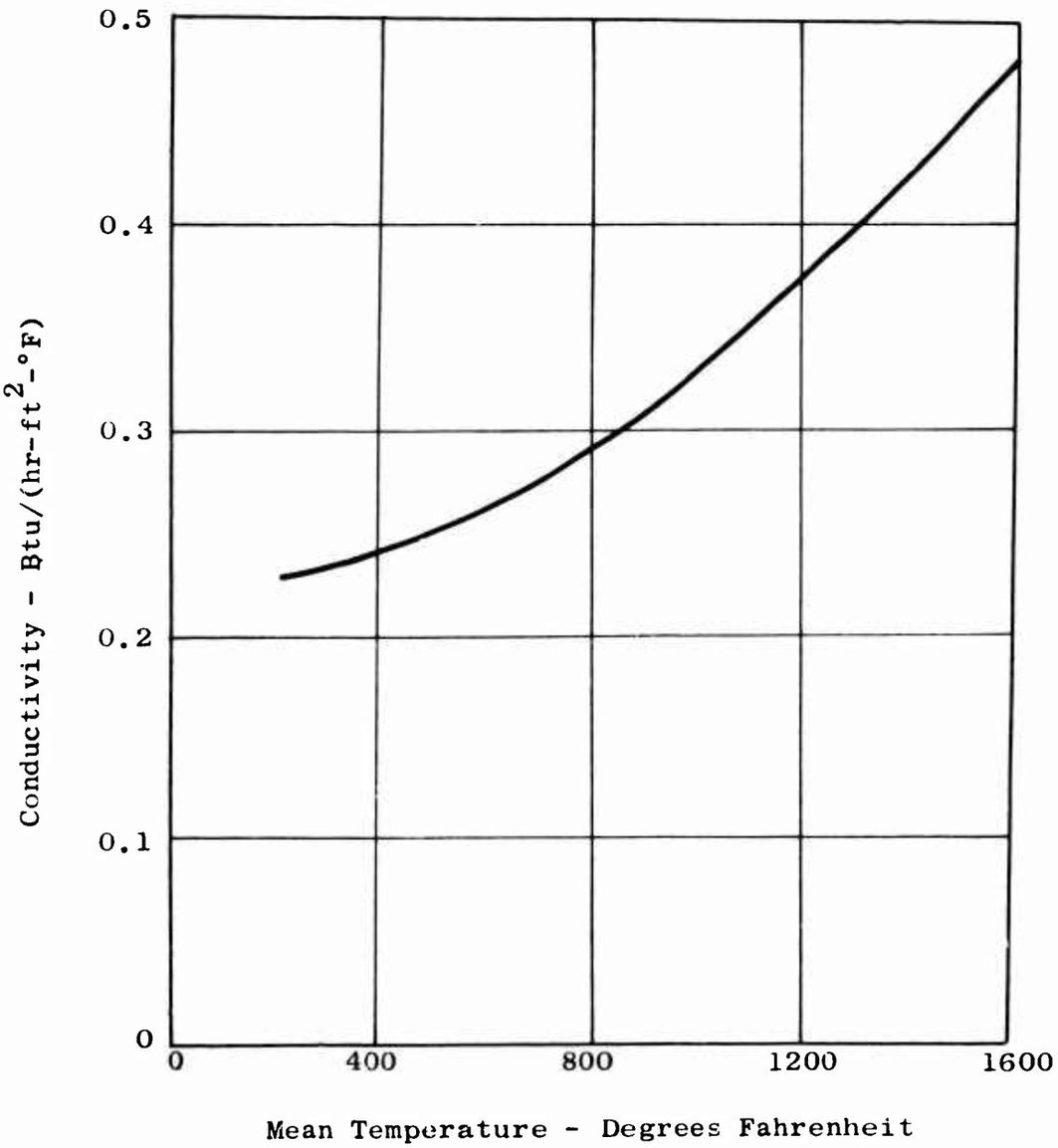

Figure 15. Thermal Conductivity of Ceramic Fiber Insulation Used in Duct Weight Analysis.

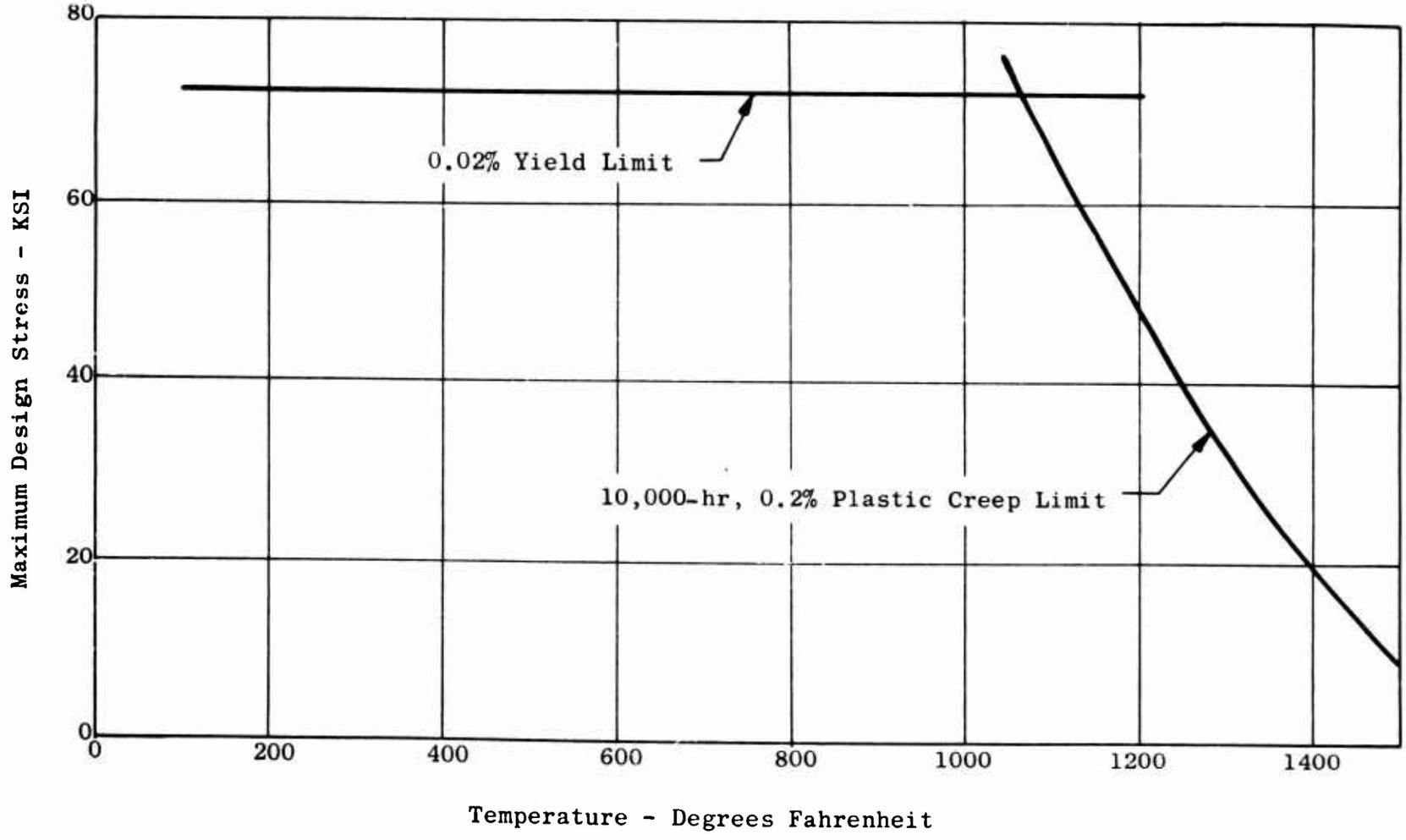

Figure 16. Design Stress for Rene′ 41 Sheet Used for Duct Analysis.

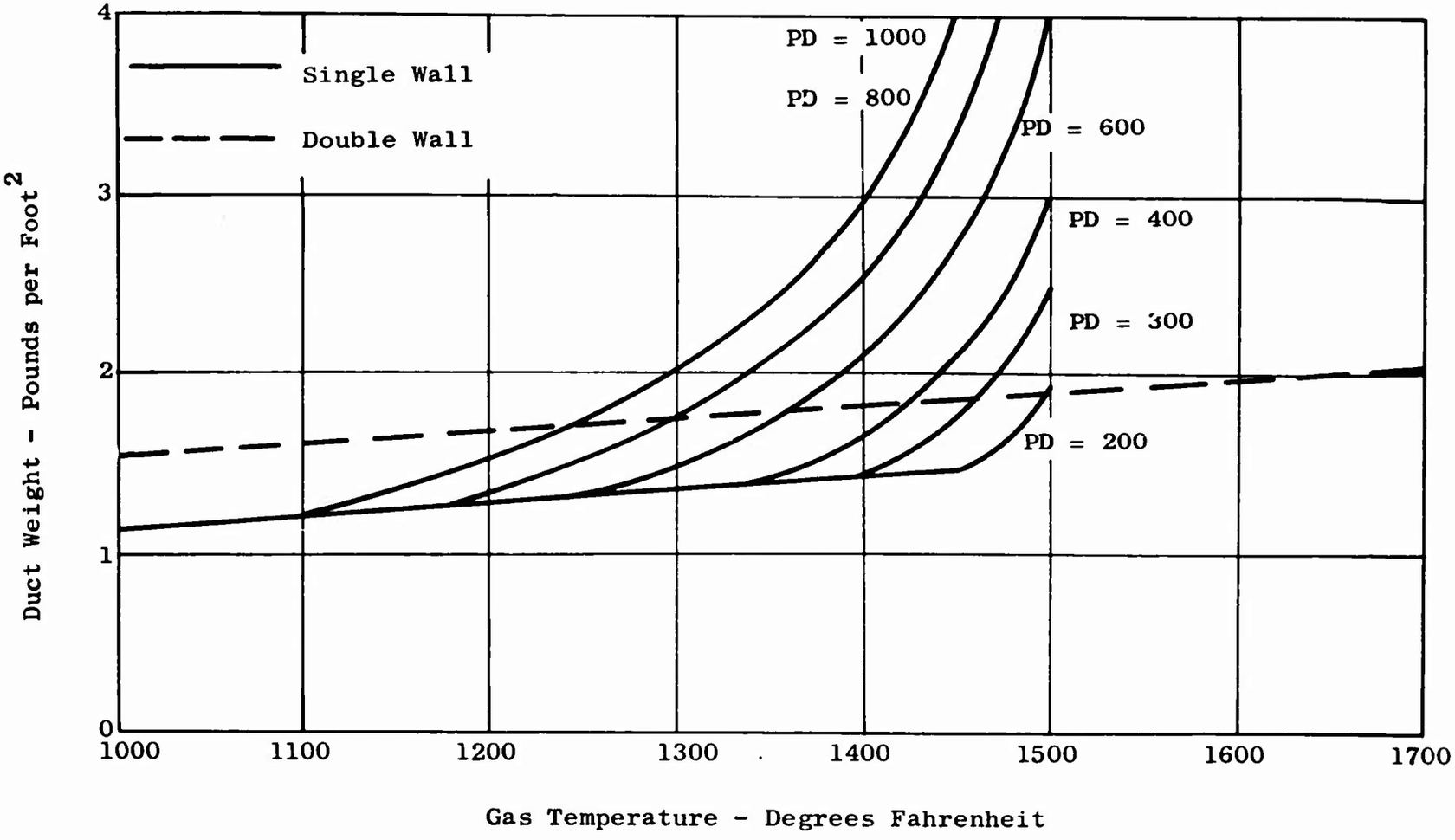

Figure 17. Ducting Weight Versus Gas Temperature for 0.015-Inch Minimum Wall Thickness.

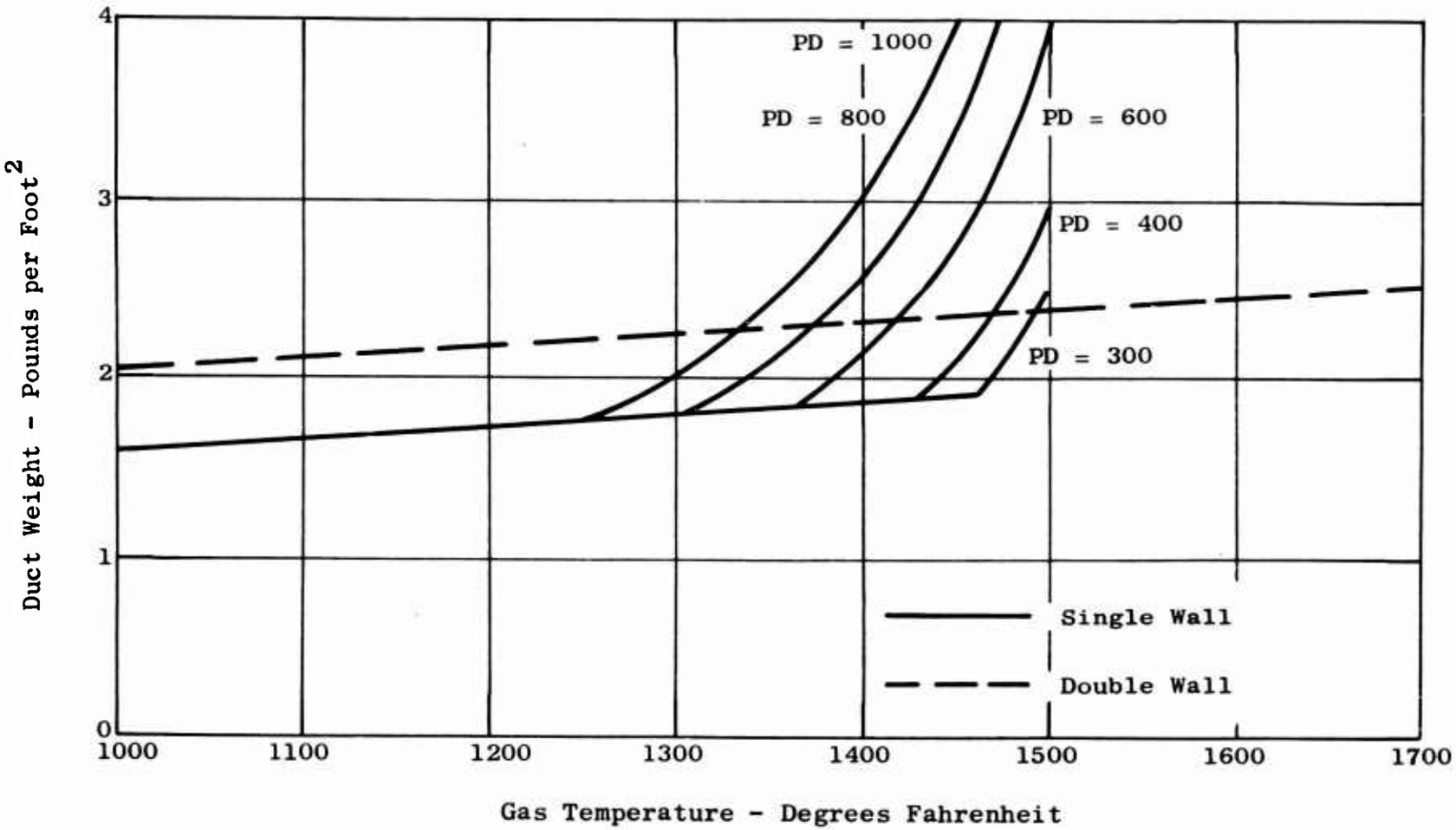

Figure 18. Ducting Weight Versus Gas Temperature for 0.025-Inch Minimum Wall Thickness.

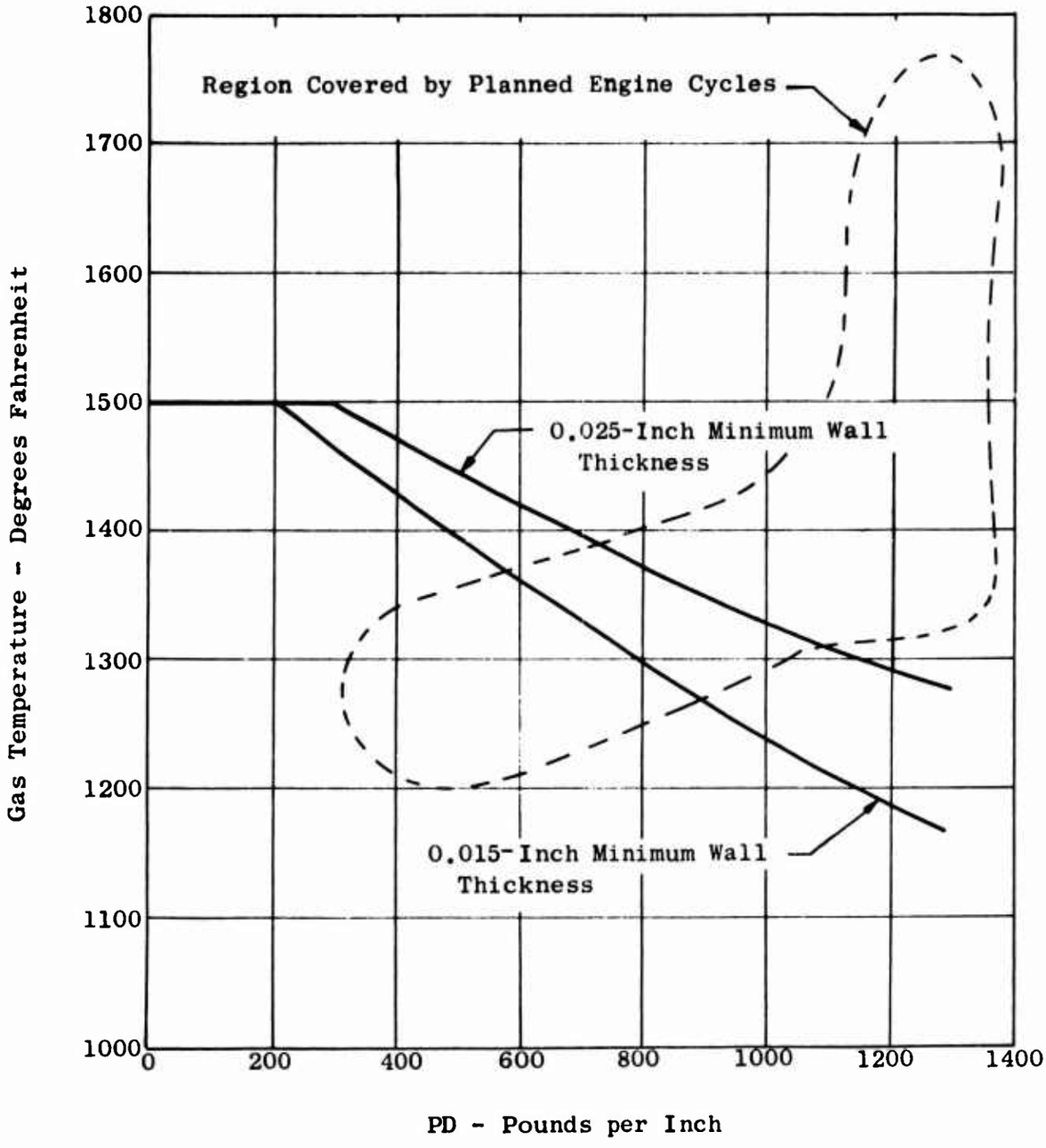

Figure 19. Gas Temperatures at Which Single-Wall and Double-Wall Ducts Are Equal Versus Product of Internal Pressure Times Diameter.

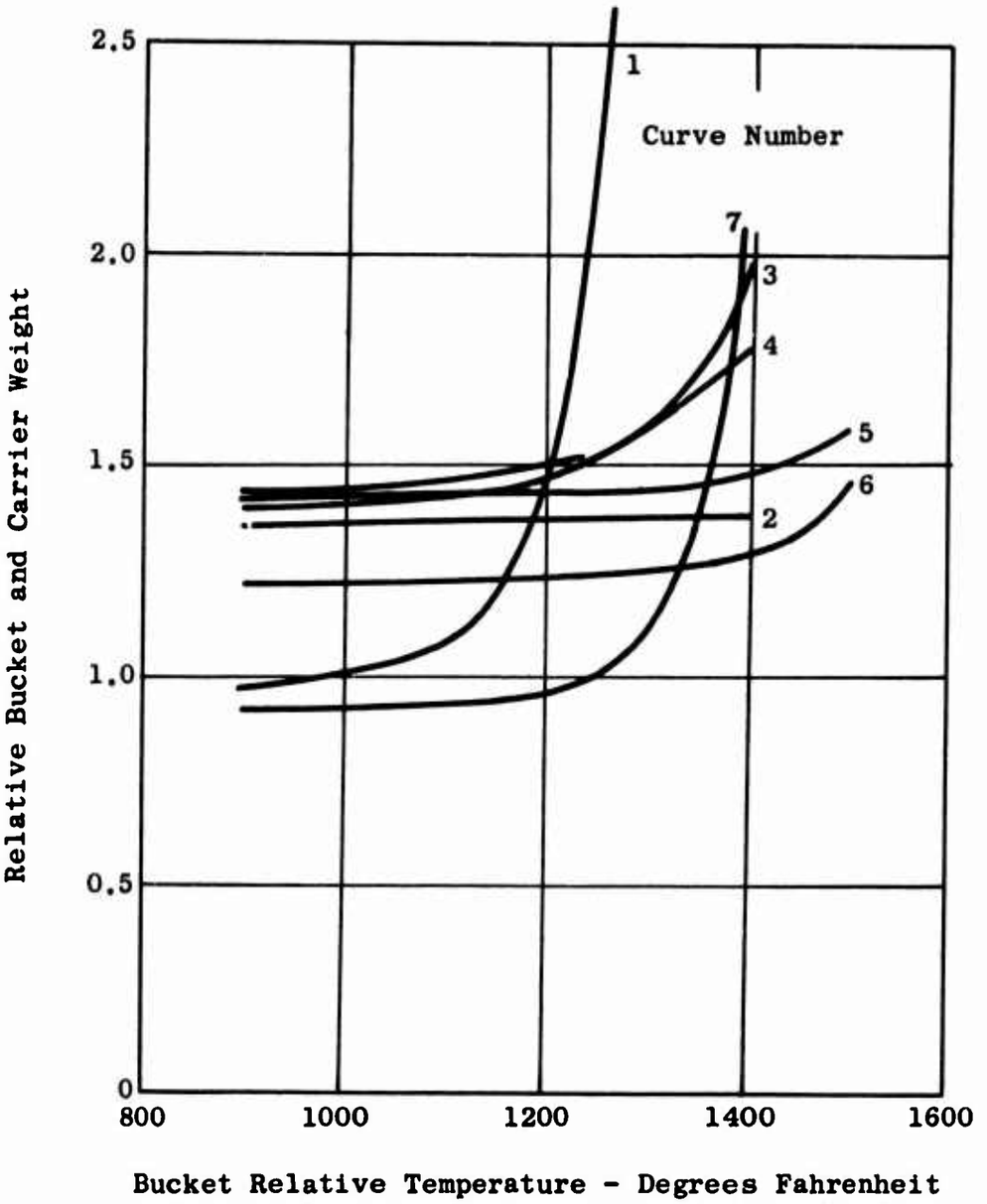

Figure 20. Effect of Cooling on Relative Bucket and Carrier Weights. (Curves are identified on pages 18 and 19.)

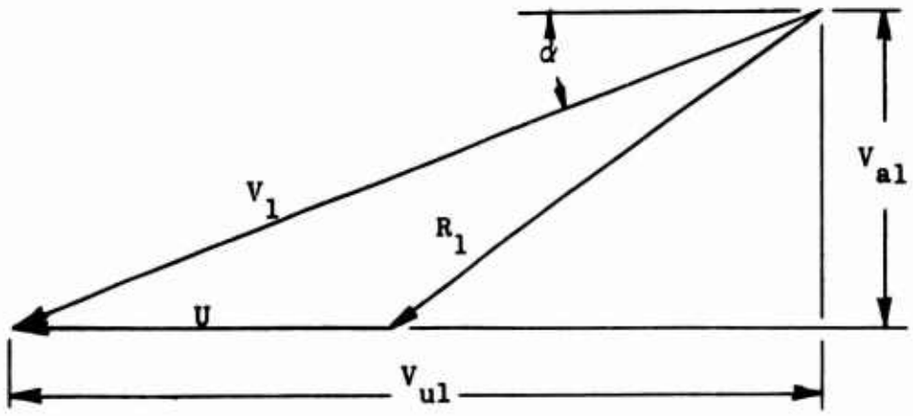

V_1 = nozzle exit gas velocity

U = bucket peripheral velocity

R_1 = bucket relative gas velocity

Figure 21. Turbine Vector Diagram at Bucket Entrance.

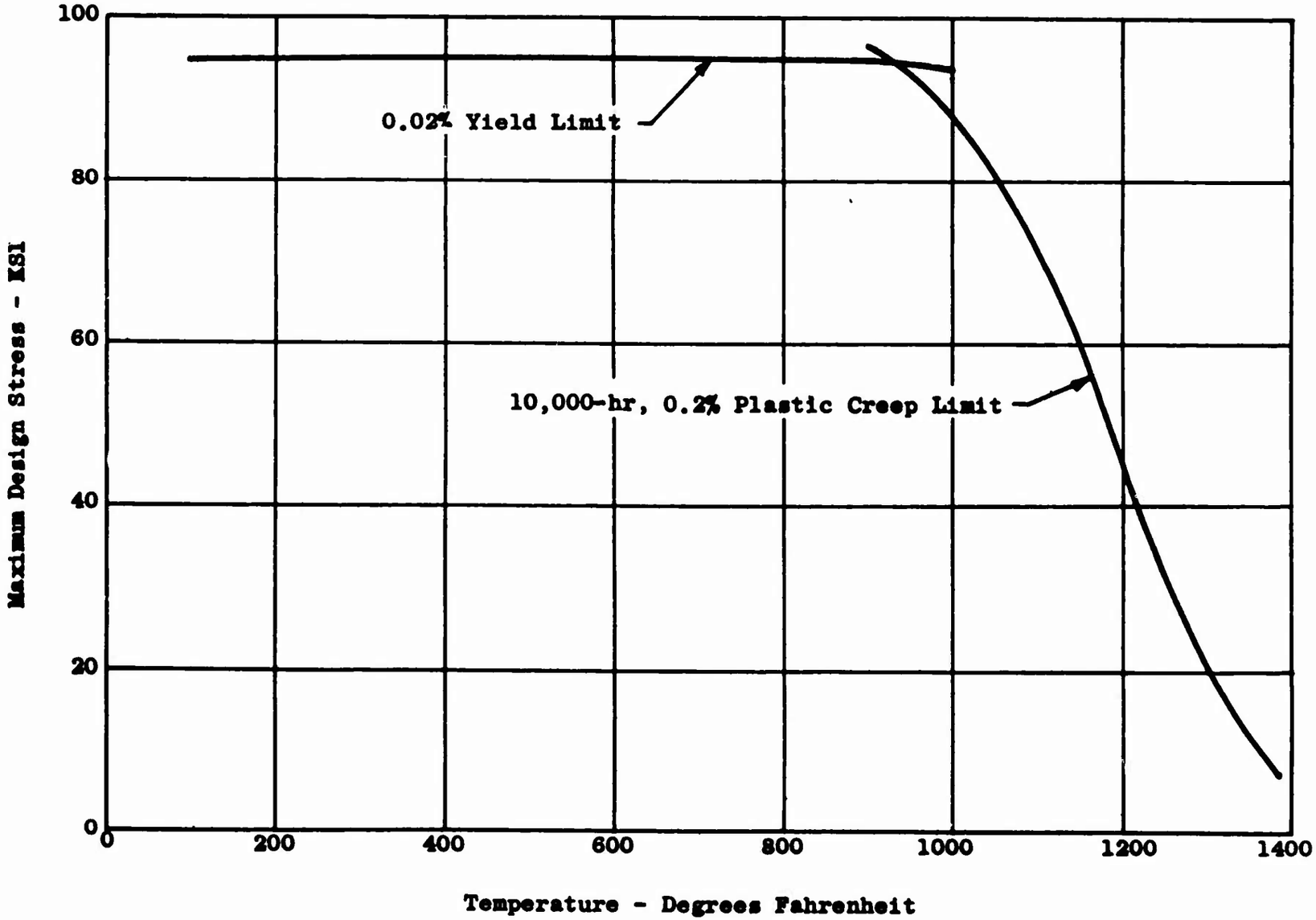

Figure 22. Design Stress for Rene' 41 Sheet Used for Carrier Analysis.

Figure 23. Design Stress for Titanium Used in Tip Tang Analysis.

UNCLASSIFIED

Security Classification

DOCUMENT CONTROL DATA - R&D

(Security classification of title, body of abstract and indexing annotation must be entered when the overall report is classified)

1 ORIGINATING ACTIVITY *(Corporate author)* General Electric Company Flight Propulsion Division Cincinnati, Ohio	2a REPORT SECURITY CLASSIFICATION 2b GROUP

3 REPORT TITLE

Investigation of High Gas Temperature Utilization for Advanced Tip Turbine Fans.

4 DESCRIPTIVE NOTES *(Type of report and inclusive dates)*

5 AUTHOR(S) *(Last name, first name, initial)*

Simonson, Marvin R.

6 REPORT DATE	7a TOTAL NO. OF PAGES	7b NO. OF REFS
August 1966	64	4

8a CONTRACT OR GRANT NO.	9a ORIGINATOR'S REPORT NUMBER(S)
DA 44-177-AMC-218(T) b. PROJECT NO. Task 1M121401D14415 c. d.	USAAVLABS Technical Report 66-37 9b OTHER REPORT NO(S) *(Any other numbers that may be assigned this report)* General Electric Company Report R66FPD198

10 AVAILABILITY/LIMITATION NOTICES

Distribution of this document is unlimited.

11 SUPPLEMENTARY NOTES	12 SPONSORING MILITARY ACTIVITY
	U.S. Army Aviation Materiel Laboratories Ft. Eustis, Virginia

13 ABSTRACT

Report discusses conceptual design studies of tip turbine fan cooling systems for compatibility with advanced high energy core engines. Work involved Phase II of U.S. Army Aviation Materiel Laboratories Contract DA 44-177-AMC-218(T): "Parametric and Preliminary Design Studies of High and Low Speed Cruise Fan Propulsion Systems". Phase I results are reported in General Electric Company Report Numbers R65FPD217 and 218.

DD FORM 1 JAN 64 1473

UNCLASSIFIED

Security Classification

14. KEY WORDS	LINK A		LINK B		LINK C	
	ROLE	WT	ROLE	WT	ROLE	WT

INSTRUCTIONS

1. ORIGINATING ACTIVITY: Enter the name and address of the contractor, subcontractor, grantee, Department of Defense activity or other organization *(corporate author)* issuing the report.

2a. REPORT SECURITY CLASSIFICATION: Enter the overall security classification of the report. Indicate whether "Restricted Data" is included. Marking is to be in accordance with appropriate security regulations.

2b. GROUP: Automatic downgrading is specified in DoD Directive 5200.10 and Armed Forces Industrial Manual. Enter the group number. Also, when applicable, show that optional markings have been used for Group 3 and Group 4 as authorized.

3. REPORT TITLE: Enter the complete report title in all capital letters. Titles in all cases should be unclassified. If a meaningful title cannot be selected without classification, show title classification in all capitals in parenthesis immediately following the title.

4. DESCRIPTIVE NOTES: If appropriate, enter the type of report, e.g., interim, progress, summary, annual, or final. Give the inclusive dates when a specific reporting period is covered.

5. AUTHOR(S): Enter the name(s) of author(s) as shown on or in the report. Enter last name, first name, middle initial. If military, show rank and branch of service. The name of the principal author is an absolute minimum requirement.

6. REPORT DATE: Enter the date of the report as day, month, year; or month, year. If more than one date appears on the report, use date of publication.

7a. TOTAL NUMBER OF PAGES: The total page count should follow normal pagination procedures, i.e., enter the number of pages containing information.

7b. NUMBER OF REFERENCES: Enter the total number of references cited in the report.

8a. CONTRACT OR GRANT NUMBER: If appropriate, enter the applicable number of the contract or grant under which the report was written.

8b, 8c, & 8d. PROJECT NUMBER: Enter the appropriate military department identification, such as project number, subproject number, system numbers, task number, etc.

9a. ORIGINATOR'S REPORT NUMBER(S): Enter the official report number by which the document will be identified and controlled by the originating activity. This number must be unique to this report.

9b. OTHER REPORT NUMBER(S): If the report has been assigned any other report numbers *(either by the originator or by the sponsor)*, also enter this number(s).

10. AVAILABILITY/LIMITATION NOTICES: Enter any limitations on further dissemination of the report, other than those imposed by security classification, using standard statements such as:

(1) "Qualified requesters may obtain copies of this report from DDC."

(2) "Foreign announcement and dissemination of this report by DDC is not authorized."

(3) "U. S. Government agencies may obtain copies of this report directly from DDC. Other qualified DDC users shall request through _____."

(4) "U. S. military agencies may obtain copies of this report directly from DDC. Other qualified users shall request through _____."

(5) "All distribution of this report is controlled. Qualified DDC users shall request through _____."

If the report has been furnished to the Office of Technical Services, Department of Commerce, for sale to the public, indicate this fact and enter the price, if known.

11. SUPPLEMENTARY NOTES: Use for additional explanatory notes.

12. SPONSORING MILITARY ACTIVITY: Enter the name of the departmental project office or laboratory sponsoring *(paying for)* the research and development. Include address.

13. ABSTRACT: Enter an abstract giving a brief and factual summary of the document indicative of the report, even though it may also appear elsewhere in the body of the technical report. If additional space is required, a continuation sheet shall be attached.

It is highly desirable that the abstract of classified reports be unclassified. Each paragraph of the abstract shall end with an indication of the military security classification of the information in the paragraph, represented as *(TS)*, *(S)*, *(C)*, or *(U)*.

There is no limitation on the length of the abstract. However, the suggested length is from 150 to 225 words.

14. KEY WORDS: Key words are technically meaningful terms or short phrases that characterize a report and may be used as index entries for cataloging the report. Key words must be selected so that no security classification is required. Identifiers, such as equipment model designation, trade name, military project code name, geographic location, may be used as key words but will be followed by an indication of technical context. The assignment of links, rules, and weights is optional.